

Journal Pre-proof

Mucoadhesive nanoparticles based on ROS activated gambogic acid prodrug for safe and efficient intravesical instillation chemotherapy of bladder cancer

Xin Xu, Kunpeng Liu, Binbin Jiao, Kejun Luo, Jian Ren, Guan Zhang, Qingsong Yu, Zhihua Gan



PII: S0168-3659(20)30180-2

DOI: <https://doi.org/10.1016/j.jconrel.2020.03.028>

Reference: COREL 10230

To appear in: *Journal of Controlled Release*

Received date: 11 November 2019

Revised date: 10 March 2020

Accepted date: 19 March 2020

Please cite this article as: X. Xu, K. Liu, B. Jiao, et al., Mucoadhesive nanoparticles based on ROS activated gambogic acid prodrug for safe and efficient intravesical instillation chemotherapy of bladder cancer, *Journal of Controlled Release* (2020), <https://doi.org/10.1016/j.jconrel.2020.03.028>

This is a PDF file of an article that has undergone enhancements after acceptance, such as the addition of a cover page and metadata, and formatting for readability, but it is not yet the definitive version of record. This version will undergo additional copyediting, typesetting and review before it is published in its final form, but we are providing this version to give early visibility of the article. Please note that, during the production process, errors may be discovered which could affect the content, and all legal disclaimers that apply to the journal pertain.

© 2020 Published by Elsevier.

Mucoadhesive nanoparticles based on ROS activated gambogic acid prodrug for safe and efficient intravesical instillation chemotherapy of bladder cancer

Xin Xu,^{a,#} Kunpeng Liu,^{b,c,e,#} Binbin Jiao,^{a,h} Kejun Luo,^{b,c,e} Jian Ren,^a Guan Zhang,^{a,g,h,*} Qingsong Yu,^{b,c,d,e,f,*} Zihua Gan^{b,c,d,e,f,*}

^aDepartment of Urology, China-Japan Friendship Hospital, Beijing, China, 100029;

^bThe State Key Laboratory of Organic–inorganic Composites, Beijing University of Chemical Technology, Beijing, China, 100029;

^cBeijing Laboratory of Biomedical Materials, Beijing University of Chemical Technology, Beijing, China, 100029;

^dBeijing Advanced Innovation Center for Soft Matter Science and Engineering, Beijing University of Chemical Technology, Beijing, China, 100029;

^eCollege of Life Science and Technology, Beijing University of Chemical Technology, Beijing, China, 100029;

^fKey Laboratory of Biomedical Materials of Natural Macromolecules (Beijing University of Chemical Technology), Ministry of Education, Beijing, China, 100029;

^gGraduate School of Peking Union Medical College and Chinese Academy of Medical Sciences, China-Japan Friendship Hospital, Beijing, China, 100029;

^hPeking University China-Japan Friendship School Clinical Medicine, Beijing, China, 100029.

These authors contributed equally to this work.

*Corresponding author. E-mail address: gzhang40@hotmail.com (Guan Zhang); yuqs@mail.buct.edu.cn (Qingsong Yu), zhgan@mail.buct.edu.cn (Zihua Gan).

Abstract

Chemotherapy is the standard of care for bladder cancer after transurethral resection of the tumor. However, the rapid excretion of clinically used formulations of anticancer drugs make the common intravesical instillation chemotherapy far from efficient. Therefore, improving the muco-adhesion and penetrability of chemotherapeutic drugs became the key factors in the post-surgery treatment of

superficial bladder cancers. Here, a reduction sensitive vehicle was developed to deliver the reactive oxygen species activated prodrug of gambogic acid for treatment of orthotopic bladder cancer. The positively charged chitosan can significantly enhance the adhesion and permeability of prodrug within the bladder wall. Moreover, by utilizing the different glutathione and ROS level between cancer cells and normal cells, the dual responsive nanoparticle can selectively and rapidly deliver drug in bladder cancer cells, and thus can significantly inhibit the proliferation of bladder cancer cells in an orthotopic superficial bladder cancer model without causing damage to normal cells. This work demonstrates that the smart prodrug nanomedicine may act as a promising drug-delivery system for local chemotherapy of bladder cancer with unprecedented clinical benefits.

Keywords: Bladder cancer, intravesical instillation chemotherapy, mucoadhesive, stimuli-responsive, prodrug

1. Introduction

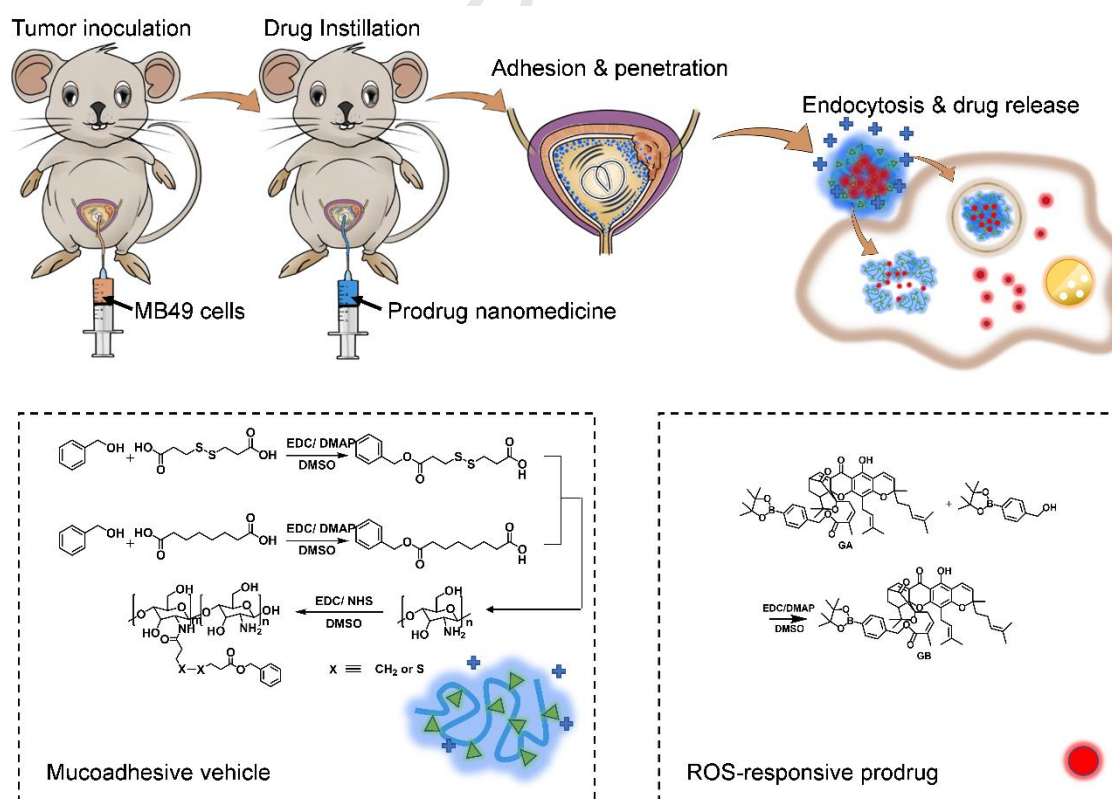
Bladder cancer (BC), approximately 75% of which was diagnosed as non-muscle-invasive type (NMIBC), [1, 2] is one of the most common malignancies worldwide. [3, 4] The mainstay standard of care for NMIBC management is transurethral resection of bladder tumor (TURBT), with an 80% early success rate. [5] However, after TURBT, many patients will experience a 50% risk of recurrence and 20% chance of progression within 5 years. [6] Because of the special physiological structure of bladder cavity, post-surgery intravesical instillation chemotherapy (IIC) can be directly administrated through the urethra to attain high local concentrations and minimal systemic toxicity. [7, 8] This could reduce the recurrence rate of NMIBC by 15-20%, and reduce the long-term recurrence rate by about 5%. [9, 10]

Although chemotherapy plays an important role in the treatment of BC, some characteristics of bladder present challenges for IIC. Firstly, the bladder permeability barrier (BPB) lining the luminal surface of the bladder prevents the efficient penetration of drugs into tumors. [7] Secondly, the residence of free drugs inside

bladder is quite short due to the voiding of urine,[11, 12] so that continuous infusion is required to maintain high drug concentration, which may result in increased expense, elevated side effects and occurrence of drug-resistance. To address these issues, various nanoscopic drug delivery vehicles have been applied, such as polymer-drug conjugates,[13] carbon nanotubes,[14] liposomes,[15, 16] polymeric nanoparticles,[17-19] nanogel,[20, 21] and so forth. Two major strategies have been applied in the development of nano-vehicles aiming at intravesical delivery of anticancer drugs. One is the introduction of active targeting moieties, for example, RGD peptide[22] and folic acid,[23, 24] which have been proved to selectively target BC cells. The other is the application of mucoadhesive materials in the construction of drug carriers, such as chitosan and its derivatives,[25, 26] polyethylene glycol,[27] hyaluronic acid,[28] alginate,[29] gelatin,[30] cationic polypeptides[20, 31] and fluorinated polyethylenimine,[32] thiolated particles,[33, 34] etc.

With these advanced nanotechnologies, the therapeutic efficacy of IIC has been greatly improved. However, the payloads of most current nanomedicines are general cytotoxic drugs like doxorubicin,[22] paclitaxel,[35] cisplatin,[36] mitomycin[19] or gemcitabine.[26] Their limitations in selectivity will inevitably be passed on to the formulated nanomedicine, which may cause the damage of normal urothelium and urethra, and further increase the risk of infection and urethral obstruction[37]. Therefore, it is essential to develop a new drug delivery system with high selectivity. Even though BC-selective peptide based nanomedicine, which resulted in great therapeutic efficacies including the prolonged lifetime and the delayed tumor growth, has been reported recently,[32] tumor-selective nanomedicine based on small molecule chemotherapeutics has merely been mentioned. In response to this demand, the increased numbers of reactive oxygen species (ROS), one characteristic of cancer cells that distinguishes themselves from normal cells,[38, 39] underlie the design criteria of efficient tumor-specific nanomedicines. Moreover, Given the different metabolic pathways and rates of cancer cells in comparison with normal ones, the high intracellular glutathione (GSH) concentration of about 10.0 mM[40, 41] in malignant cells also provide an interesting target.

Herein, based on the above considerations, a new GSH responsive delivery system based on positively charged chitosan, a well-established mucoadhesive biomolecule used as a drug carrier for enhancing the contact between drugs and bladder for better tissue permeability and longer residence time,[42] was developed to deliver ROS activated gambogic acid prodrug (noted as GB). Gambogic acid (GA), a naturally occurring xanthone-based moiety, extracted from *Garcinia hanburyi* tree, is known to be an efficient anticancer drug through numerous intracellular and extracellular actions, including programmed cell death, autophagy, cell cycle arrest, anti-angiogenesis, anti-metastatic, and anti-inflammatory activities.[43] In this way, drug release can only be triggered by the higher concentration of GSH and ROS level inside BC cells, which will then exempt normal urothelium. To verify our hypothesis, the solution properties, drug release profiles, in vitro activity and selectivity has been investigated. Meanwhile, an orthotopic BC xenograft model was established to evaluate the anticancer efficacy and safety profiles.



Scheme 1. The schematic illustration of intravesical instillation of tumor cells or various drugs and the synthetic routes of vehicle and prodrug.

2. Materials and methods

2.1 Materials

Gambogic acid was purchased from Sichuan Weikeqi Biological Technology Co. Ltd. 4-Dimethylaminopyridine (DMAP), N-hydroxy succinimide (NHS), dicyclohexyl carbodiimide (DCC), 1-(3-dimethylaminopropyl)-3-ethylcarbodiimide hydrochloride (EDC), 4-hydroxybenzylboronic acid pinacol ester, chitosan (Mw=5kDa), 4,4'-dithiodipropionic acid, adipic acid, benzyl alcohol, dihydroethidium, anhydrous dimethylsulfoxide (DMSO) were purchased from Aladdin and used without further purification. Mouse BC cells (MB49) and mouse fibroblasts (NIH-3T3) were purchased from cell bank of typical culture preservation committee of Chinese Academy of Sciences. Dulbecco's modified eagle's medium (DMEM), fetal bovine serum (FBS) and penicillin/streptomycin solution were obtained from Wisent (Canada). The other chemicals (reagent grade) in this work were purchased from Sigma Aldrich and used directly.

2.2 Synthesis and characterization of ROS responsive Gambogic acid prodrug (GB)

125 mg of gambogic acid (0.2 mmol), 140 mg 4-hydroxybenzylboronic acid pinacol ester (0.6 mmol) were dissolved in 10 mL dichloromethane (DCM). 61.8 mg DCC and 10 mg DMAP were added and reacted under room temperature for 12 h. The precipitate was then filtered, the filtrate was washed with 1M HCl, saturated sodium bicarbonate, saturated sodium chloride. The organic phase was collected and dried with anhydrous sodium sulphate followed by rotary evaporation. The product was further purified through column chromatography using ethyl acetate and n-hexane (1:5) as elution phase. The final product was obtained after vacuum drying. The chemical structure of the GB was analyzed by ^1H NMR (Bruker AVANCE 400MHz).

2.3 Synthesis and characterization of hydrophobically modified chitosan

The functionalized chitosan was synthesized by two-step reaction. At the first step, dithiodipropionic acid or adipic acid was reacted with benzyl alcohol to yield dithiodipropionic acid mono benzyl ester or adipic acid mono benzyl ester. Taking dithiodipropionic acid as an example, 4.205 g dithiodipropionic acid (20 mmol) and 0.432 g benzyl alcohol (4 mmol) were firstly dissolved in 40 mL dimethylformamide.

Then 0.62 g EDC (4 mmol) and 0.049 g DMAP were added and reacted under room temperature for 12 h. DMF was removed by rotary evaporation and DCM was added to precipitate the unreacted dithiodipropionic acid. The filtrate was washed with saturated sodium chloride and dried with anhydrous sodium sulphate. The product was purified with column chromatography. The column was firstly washed with DCM:methanol (15:1) and then with DCM:methanol (10:1) to yield final product.

The second step was the amidation of chitosan with mono benzyl ester. Briefly, 1.08 g chitosan (6.7 mmol amino group) and 0.244 g dithiodipropionic acid mono benzyl ester (0.8 mmol) were dissolved in 50 mL DMF. 0.23 g EDC (1.2 mmol) and 0.138 g NHS (1.2 mmol) were then added and reacted under room temperature for 24 h. The product was purified by repeated precipitation in acetone to remove the unreacted dithiodipropionic acid mono benzyl ester. Then the precipitate was re-dissolved in DMF and dialyzed in water. The pure product dithiodipropionic acid mono benzyl ester modified chitosan (^{SS}CB) could be obtained after freeze drying.

2.4 Preparation and characterization of mucoadhesive nanoparticles

The mucoadhesive nanoparticles based on chitosan polymer were prepared by nanoprecipitation method. Briefly, taking ^{SS}CB_{GB} as an example, 10 mg ^{SS}CB and 5 mg GB was dissolved in 1 mL of DMF and slowly injected into 10 mL water with syringe pump (Langer Pump Co. Ltd.) at a flow rate of 2 mL/h. After injection, the solution was further stirred for 1 h and then dialyzed in water (MWCO = 8,000 ~ 14,000 Da).

The size and zeta potential of as-prepared nanoparticles were characterized by dynamic light scattering using Malvern Zeta sizer (ZS90, Malvern, Germany). The morphology of nanoparticles was further detected using transmission electron microscope (TEM, JEM-2100, JEOL, Japan).

2.5 Cell culture

The MB49 and NIH-3T3 cells were grown in DMEM medium supplemented with 10% FBS. Cells were maintained at 37 °C in a humidified atmosphere of 5% carbon dioxide and 95% air.

2.6 In vitro cytotoxicity assay

MB49 cells were plated in 96-well plates and treated by different amount of GA, GB, ^{CC}CB_{GA}, ^{SS}CB_{GA}, ^{CC}CB_{GB} and ^{SS}CB_{GB} for 24 h. The cytotoxicity was evaluated using the MTT [3-(4, 5-dimethylthiazol-2-yl)-2,5-diphenyl-tetrazolium bromide] cell viability assay as previously described.[44] The plates were read spectrophotometrically at 570nm using a microplate spectrophotometer (Multiskan GO, Thermo Scientific). The IC50 values were calculated by GraphPad Prism software.

2.7 Detection of apoptosis and cell cycle arrest in vitro

To measure apoptosis and cell cycle arrest caused by various drugs, MB49 cells were seeded on six-well plates at a density of 3×10^5 cells/well and cultured for 24 hours. Then GA, GB, ^{CC}CB_{GA}, ^{SS}CB_{GA}, ^{CC}CB_{GB} and ^{SS}CB_{GB} with 2 μ M GA equivalent was added and cultured for 24 hours. Cells were collected, washed twice with PBS and treated with apoptosis detection Kit and cell cycle Kit separately. Apoptotic cells and cell cycle of treated cells were then analyzed with Flow Cytometer (FCM, BD Biosciences).

2.8 Cellular uptake of responsive and non-responsive nanoparticles

To detect the cellular uptake of nanoparticles, 2% weight of DiI was added during nanoparticle fabrication. MB49 cells were seeded onto 35 mm glass bottom petri dish (NEST) at a density of 2×10^5 cells/well and cultured for 24 hours. Then medium containing 0.1 mg·mL⁻¹ DiI labeled ^{SS}CB_{GB} and ^{CC}CB_{GB} was added and cultured for 3 hours or 9 hours. The medium containing the drugs was discarded and the cell nucleus was stained with Hoechst 33342 for 15 min. Cells were observed under a confocal laser scanning microscope (CLSM, TCS SP8, Leica) after washed with PBS.

2.9 Endocytic mechanism study

Analysis of endocytic pathway of nanoparticles was conducted by flow cytometry. Briefly, MB49 cells were seeded into 6-well plates (3×10^5 cells/well) at 24 h before the experiment. The cells were pretreated for 30 min with 37°C, 4 °C, with chlorpromazine (10 μ M) to inhibit the formation of clathrin vesicles and filipin III (1 μ g/mL) to inhibit caveolae, and amiloride (50 μ M) to inhibit macropinocytosis, and

then treated with DiI labeled nanoparticles for an additional 1 h. Next, the cells were washed twice with ice cold PBS (pH 7.4) and observed with ARVOX3 multifunctional microplate reader (Perkin Elmer, Waltham, MA, USA).

2.10 Co-localization of nanoparticles with lysosomes

MB49 cells were seeded onto 35 mm glass bottom petri dish at a density of 2×10^5 cells/well and cultured for 24 hours. Then medium containing 0.1 mg/mL DiI labeled $^{CC}CB_{GB}$ and $^{SS}CB_{GB}$ nanoparticles was added and cultured for 3 hours. The cells were then washed with PBS and the nuclei and lysosome were stained with Hoechst 33342 dye and LysoTracker Green DND-26 for 15 min and 30 min, respectively. After washing with PBS, the colocalization was investigated with CLSM.

2.11 Establishment of orthotopic BC xenograft model

Female C57BL/6J mice (5-6 weeks old) were purchased from Beijing Huafukang biological Co. Ltd. All animal experiments were performed in accordance with guidelines of Peking University Health Science Center Animal Care and Use Committee under the protocols approved by the Institutional Animal Care and Use Committee at Peking University (Beijing, China). During the experiment, the animals were under isoflurane anesthesia. After the anesthesia was stable, urethral intubation (flexible tube of the 24G BD intravenous catheters) was performed on the mice. Clean the bladders with PBS buffer solution for 3 times. The mouse bladders were then infused with 0.1 mol/L HCl for 25 seconds, and then instilled with 0.1 mol/L NaOH for 5 seconds. After washing with PBS for 3 times, the bladders were infused with 0.025% trypsin solution for 10 min followed by 3 times PBS washing. To enhance the adhesive ability of MB49 cells, the bladders were instilled with 0.1 mg/mL Poly-L-lysine solution for 10 min. Finally, the mouse bladders were infused with MB49 cells suspension, and to avoid spontaneous micturition, the animals remained anesthesia for approximately 60 min after intravesical instillation.

To prove the successful establishment of orthotopic BC model, MB49 cells labeled with a membrane dye, DiR, was intravesical instilled. The in situ fluorescent signal at five days post-instillation was monitored using IVIS Spectrum in vivo living

imaging system (PerkinElmer, U.S.A). Meanwhile, the bladders were also excised and subjected to hemoxilin & eosin (H&E) staining to confirm the formation of tumor mass.

2.12 The ROS level in normal bladder and cancerous bladder

Dihydroethidium (DHE), a lipophilic probe which readily diffuses across cell membranes and be rapidly oxidized to ethidium (a red fluorescent compound) by superoxide and hydrogen peroxide (H_2O_2) (in the presence of peroxidase), was used for the measurement of intracellular ROS content. The normal and tumor bearing mice were anesthetized and sacrificed. Then the bladders were excised and stored immediately under $-80^\circ C$ for frozen section. The bladder slices were then stained cells with $5\mu M$ DHE and DAPI and observed by CLSM.

2.13 Retention of drug delivery system in the bladder of mice (In vivo fluorescence imaging)

5 days after intravesical instillation of MB49 cells, mice were randomized into 3 groups (3 mice in each group). Then $50\ \mu L$ free Cy7.5, Cy7.5 labeled $^{SS}CB_{GB}$ and $^{CC}CB_{GB}$ at $0.1\ mg/mL$ Cy7.5 concentration were infused via urethra (after anesthesia). Then the mice were placed supine on an IVIS light-tight chamber. Optical imaging of the Cy7.5 was conducted on an IVIS Spectrum in vivo imaging system using 745/800 filter combination. The exposure time were set as 10 s. The fluorescence intensity at the bladder region was quantified by Living Image version 4.4 In Vivo Imaging Software (PerkinElmer, U.S.A).

2.14 Permeability of nanoparticle in urothelium

To investigate the penetration of drug delivery system in urothelium, normal C57BL/6J mice were divided into 3 groups (3 mice in each group), and were intravesical instilled with $50\ \mu L$ of $0.1\ mg/mL$ of free DiI or DiI labeled $^{CC}CB_{GB}$ and $^{SS}CB_{GB}$ nanoparticles. After staying for two hours under anesthesia, the flexible tube was extracted, and the fluid in mice bladder was expelled by gently pressing the abdomen of the mice. To analyze the penetration, the mice were sacrificed, then the bladders were excised and were spread out on cover slides. The penetration of fluorescence in the mucosa of bladder was observed by confocal microscope.

Furthermore, sections were also cut transversely through the midportion of the excised bladder. The fluorescence distribution in the bladder wall was investigated with CLSM.

2.15 Anticancer efficacy and in vivo safety

To investigate the tumor suppression effect of various drugs, tumor bearing mice were divided into 5 groups with 5 mice in each group. 50 μ L of GA, GB, ^{CC}CB_{GB}, ^{SS}CB_{GB} and Saline at 5mg/kg GA equivalent were instilled every three days. Mice were weighted after every instillation. After 5 times instillation, the mice were sacrificed. The bladders were excised, weighed, embedded in paraffin after fixed in 4% paraformaldehyde for 24 h, and submitted for histopathological staining. Sections were also cut transversely through the midportion of the bladder and subjected to Ki-67 and Terminal deoxynucleotidyl transferase (TdT) dUTP Nick-End Labeling (TUNEL) staining. The heart, liver, spleen, lung and kidney were excised from one mouse in each group for H&E staining to evaluate the toxicity of drug administration on normal organs.

2.16 Statistical analysis

All data were reported as averages plus/minus the standard deviation (mean \pm SD). Statistical significance was assessed by one-way ANOVA with Bonferroni post-tests using GraphPad Prism 5.0 software.

3. Results and discussion

3.1 Preparation and characterization of gambogic acid prodrug and chitosan nanoparticles

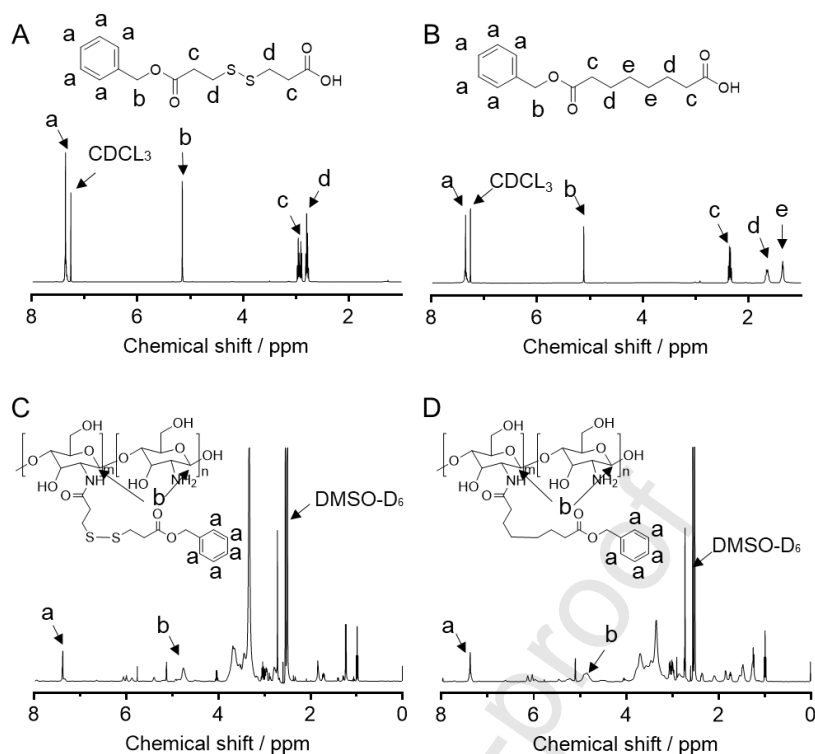


Figure 1. The ^1H NMR spectra of (A) dithiodipropionic acid mono benzyl ester, (B) adipic acid mono benzyl ester, (C) $^{\text{SS}}$ CB and (D) $^{\text{CC}}$ CB.

As a naturally originated positively charged polysaccharide, the intrinsic mucoadhesive property of chitosan make itself an ideal intravesical delivery vehicle.[45] As shown in Scheme 1, in order to efficiently encapsulate hydrophobic payloads, part of the amino groups of low molecular weight chitosan ($M_w = 5\text{kDa}$) was modified with hydrophobic moieties containing benzyl group. Benzyl alcohol was firstly reacted with 3, 3'-dithiodipropionic acid and adipic acid, respectively, to yield the GSH responsive and non-responsive intermediates. The structure of these intermediates could be confirmed by ^1H NMR spectra (Figure 1A&B). As shown in Figure 1A, the resonance at 7.39 ppm (a) could be attributed to the benzene ring. The signals at 2.96 ppm (c) and 2.87 ppm (d) could be ascribed to the protons near carbonyl group and disulfide group, respectively. The integration ratio between peak (a) and peak (c) was found to be 5:3.8, indicating the hetero-functionalization of the two acid groups. Similarly, the structure of mono-modified adipic acid could also be confirmed by the integration ratio of 5:3.8:3.9:3.9 between the signals at 7.39 ppm (a),

2.38 ppm (c), 1.76 ppm (d) and 1.55 ppm (e) in the ^1H NMR spectrum (Figure 1B). The responsive and non-responsive intermediates were then linked to chitosan to obtain responsive ($^{\text{SS}}\text{CB}_{\text{GB}}$) and non-responsive carriers ($^{\text{CC}}\text{CB}_{\text{GB}}$), respectively. The successful amidation could be proved by the presence of benzene signals in the respective ^1H NMR spectra after repeated precipitation with acetone (Figure 1C&D). The substitution degree calculated according to the integration ratio between (a) and (b) was 5.9% and 6.3% for $^{\text{SS}}\text{CB}_{\text{GB}}$ and $^{\text{CC}}\text{CB}_{\text{GB}}$, respectively.

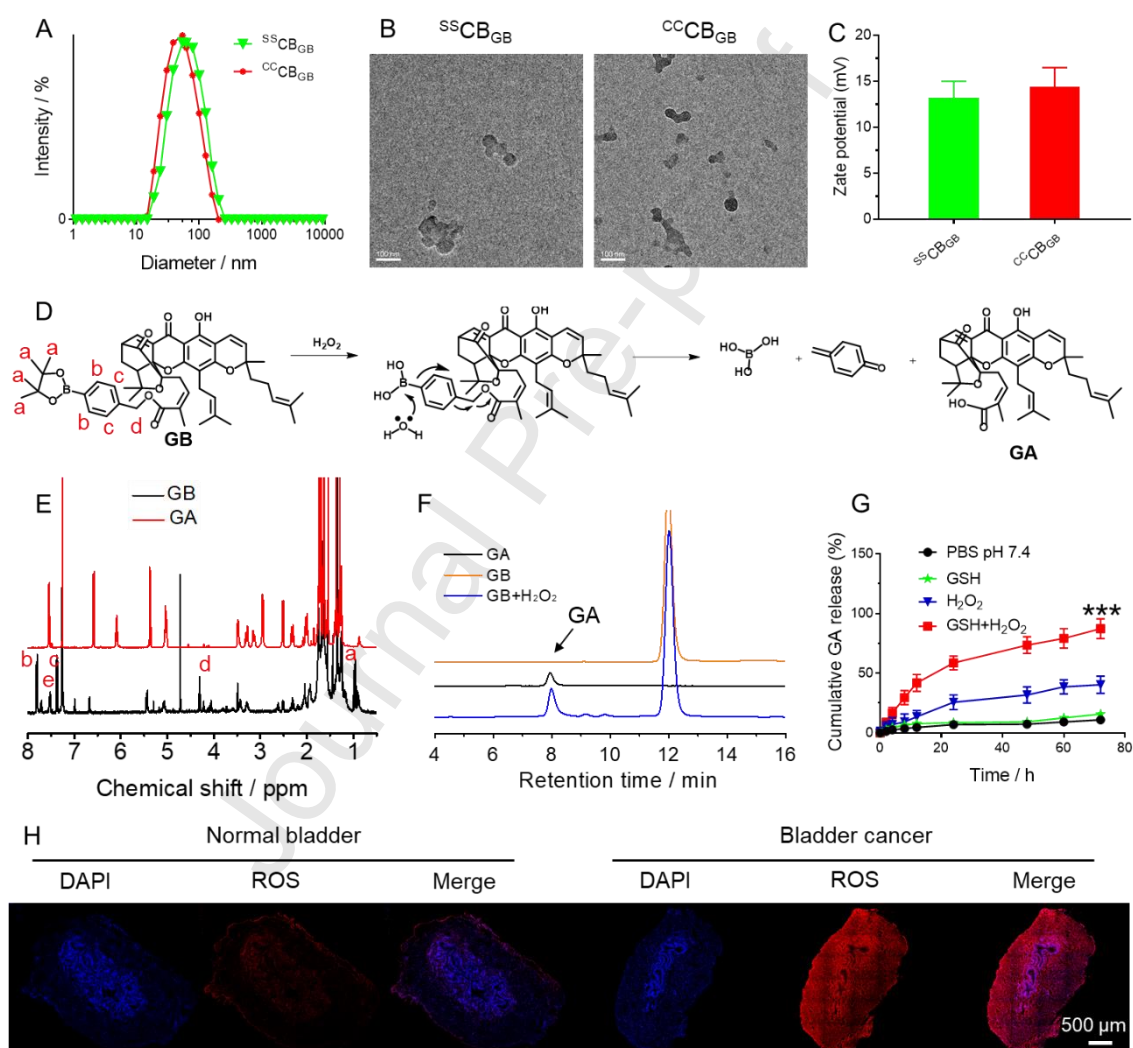


Figure 2. (A) Rh and (B) Typical TEM images of $^{\text{SS}}\text{CB}_{\text{GB}}$ and $^{\text{CC}}\text{CB}_{\text{GB}}$ nanoparticles, scale bar represents 100 nm. (C) Zeta potential of $^{\text{SS}}\text{CB}_{\text{GB}}$ and $^{\text{CC}}\text{CB}_{\text{GB}}$ in 10 mM PBS (pH 7.4). (D) The speculative ROS activate mechanism of GB prodrug. (E) The ^1H NMR spectra of GA and GB. (F) The HPLC elution curves of GA, GB and GB plus H_2O_2 . (G) Release profiles of GA from $^{\text{SS}}\text{CB}_{\text{GB}}$ nanoparticle under different

conditions (***) $p < 0.001$ for GSH + H₂O₂ group compared with the other groups. All the statistical data are represented as mean \pm SD (n=3). (H) ROS level in normal bladder and cancerous bladder. Cell nucleus were stained by DAPI (in blue), ROS was stained by DHE (in red).

Intracellular ROS signaling including H₂O₂, superoxide anions (O₂⁻) and hydroxyl radicals are known to be elevated in cancerous cells[46] and capable of oxidizing benzylboronic acid/esters[47, 48] to trigger drug release[49] or activation of prodrugs.[50] Therefore, in order to achieve selective inhibition of cancer cells, a ROS responsive prodrug GB was synthesized by the esterification between GA and 4-(hydroxymethyl) benzylboronic acid pinacol ester. As shown in Figure 2E, the chemical structure of GB could be confirmed by the presence of 4-(hydroxymethyl) benzene boronic acid pinacol ester signals and the integration ratio of 2:1.08 between peak (b) and peak (c) in the ¹H NMR spectrum. GB prodrug were then loaded by ^{SS}CB or ^{CC}CB to form ^{SS}CB_{GB} and ^{CC}CB_{GB} nanoparticles through nanoprecipitation method. The DLC and DLE reached relatively high levels, that is, 36.7% and 73.5% for ^{SS}CB_{GB} and 35.8% and 71.8% for ^{CC}CB_{GB}. The resulted ^{SS}CB_{GB} and ^{CC}CB_{GB} nanoparticles exhibited spherical morphology under TEM (Figure 2B). The average diameters of ^{SS}CB_{GB} and ^{CC}CB_{GB} were 83.4 nm (PDI=0.183) and 78.8 nm (PDI=0.207), respectively, as determined by DLS (Figure 2A), which were slightly larger than that obtained from TEM, possibly due to the dehydration. Because the nanoparticles were administered after voiding of bladder, the stability of nanoparticle was evaluated in PBS only, in which stable size could be obtained during 7 days incubation (Figure S1). Notably, due to the positive nature of chitosan, both ^{SS}CB_{GB} and ^{CC}CB_{GB} nanoparticles were positively charged in PBS at pH 7.4 with zeta potential of 12.3 \pm 1.1 mV and 13.1 \pm 1.2 mV (Figure 2C), which may facilitate the interaction between nanoparticles and biological membranes.

To evaluate whether GB prodrug could be transformed into GA by ROS activation. GB prodrug was co-incubated with 1 mM H₂O₂ at pH 7.4 for 1 h, then the products were analyzed with HPLC. As shown in Figure 2F, compared with GB, a

new peak corresponding to GA appeared after treatment, indicating the successful transformation of GB. The *in vitro* release behaviors of ^{SS}CB_{GB} and ^{CC}CB_{GB} nanoparticles were investigated in PBS (pH 7.4) with or without 10mM GSH or 1mM H₂O₂. As shown in Figure 2G, GA could be efficiently released in the presence of both 10mM GSH and 1mM H₂O₂, with a total 78.4% of GA detected at 72h by HPLC. In contrast, without GSH, 27.8% of GA could be released, while without H₂O₂, only trace amount of free GA could be detected, indicating that the rapid GA release could only be triggered by the presence of both high level GSH and H₂O₂ inside cells. Moreover, the dual-sensitivity of ^{SS}CB_{GB} could also be proved by the release profiles of ^{CC}CB_{GB} nanoparticles under the same conditions (Figure S2), in which much slower release rate were observed even in the presence of both GSH and H₂O₂. Considering the higher ROS level in cancerous tissues, as showed by the stronger red fluorescence in cancerous bladder compared with the normal bladder (Figure 2H), the ROS- and GSH- dual responsiveness of as-prepared prodrug nanomedicine may predict higher toxicity in cancer cells.

3.2 Cellular uptake, intracellular transportation and cytotoxicity of prodrug nanomedicine

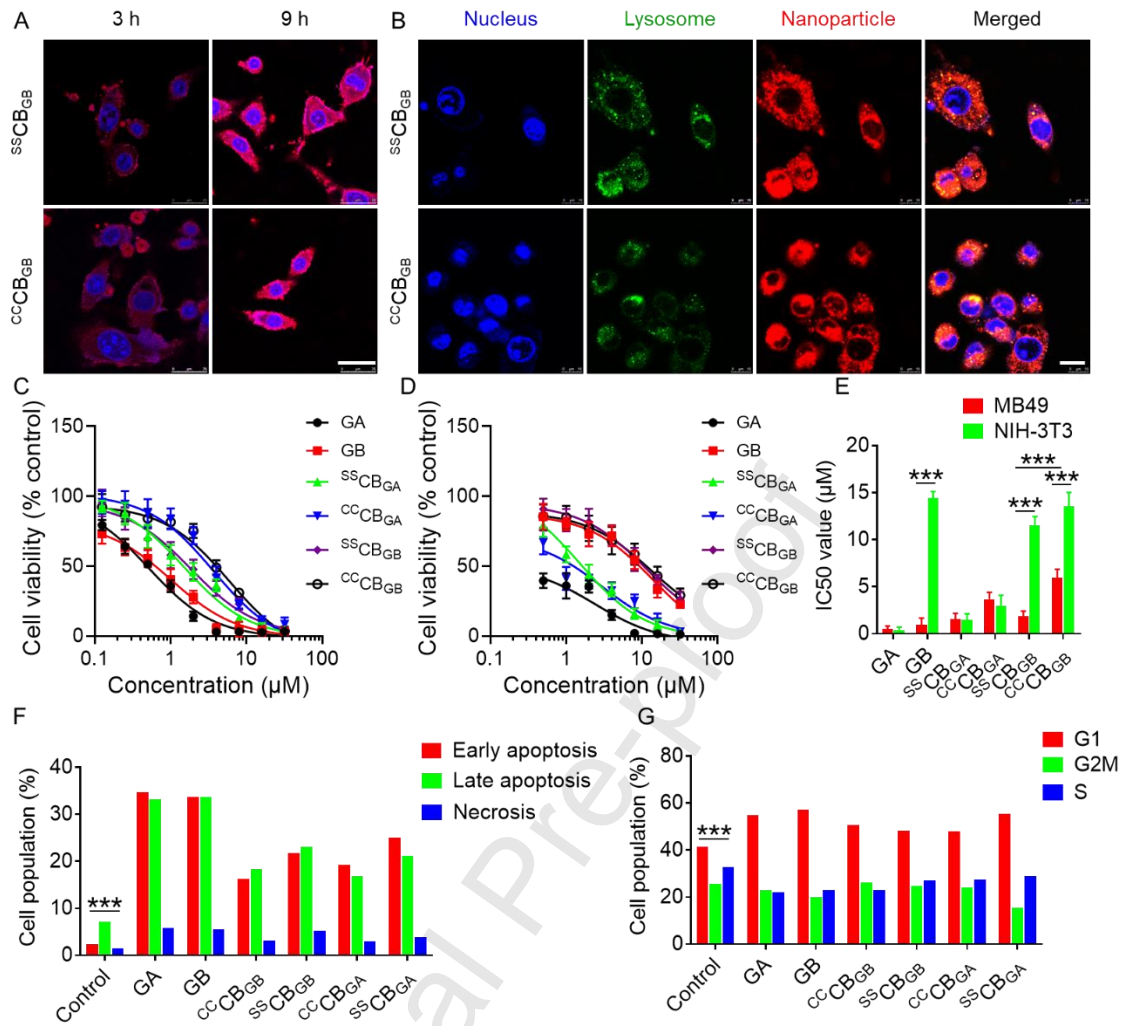


Figure 3. (A) The cellular uptake of DiI labeled $^{SS}CB_{GB}$ and $^{CC}CB_{GB}$ nanoparticles (red) at 3 h and 9 h after co-incubation, the nuclei were stained with Hoechst 33344 (blue). (B) The colocalization between DiI labeled $^{SS}CB_{GB}$ and $^{CC}CB_{GB}$ nanoparticles (red) with lysosome (green). The in vitro cytotoxicity of GA, GB, $^{CC}CB_{GA}$, $^{SS}CB_{GA}$, $^{CC}CB_{GB}$ and $^{SS}CB_{GB}$ after co-incubation with (C) MB49 cells and (D) NIH-3T3 cells for 24 h. Data are presented as mean \pm SD (n=6). (E) The IC50 values of GA, GB, $^{CC}CB_{GA}$, $^{SS}CB_{GA}$, $^{CC}CB_{GB}$ and $^{SS}CB_{GB}$ against MB49 and NIH-3T3 cells (***P<0.001 for MB49 cells compared with NIH-3T3 cells). (F) The pro-apoptotic ability and (G) cell cycle arrest capacity of Saline, GA, GB, $^{CC}CB_{GA}$, $^{SS}CB_{GA}$, $^{CC}CB_{GB}$ and $^{SS}CB_{GB}$ (**p<0.001 for saline group compared with the other groups).

The internalization of $^{SS}CB_{GB}$ and $^{CC}CB_{GB}$ nanoparticles by MB49 cells were

monitored with CLSM. For CLSM observation, MB49 cells were incubated with 100 $\mu\text{g/mL}$ DiI labeled $^{SS}\text{CB}_{\text{GB}}$ and $^{CC}\text{CB}_{\text{GB}}$ nanoparticles for 3 or 9 h. As depicted in Figure 3A, after 3 h co-incubation, red fluorescence of DiI was observed both on the membrane and inside cells. Markedly enhanced fluorescence was observed at 9 h, indicating the time-dependent uptake kinetics. The membrane bounded fluorescence at both 3 and 9 h might be attributed to the electrostatic interaction between positively charged chitosan and the membrane. The endocytic mechanism study was carried out by pre-incubating MB49 cells under different conditions (4 °C, 37 °C) or in the presence of various endocytosis inhibitors (such as chlorpromazine (CPZ), filipin III (Fil), and amiloride (Amil)).[51] The cellular fluorescence was evaluated using multifunctional microplate reader (Figure S4). It could be found that the endocytosis of nanoparticles by MB49 cells was energy dependent and mediated by multiple mechanisms. The colocalization study of $^{SS}\text{CB}_{\text{GB}}$ and $^{CC}\text{CB}_{\text{GB}}$ nanoparticles with lysosome was carried out after 6 h co-incubation. As shown in Figure 3B, both $^{SS}\text{CB}_{\text{GB}}$ and $^{CC}\text{CB}_{\text{GB}}$ nanoparticles were found to partially colocalized with Lysosome, corroborating that multiple endocytic pathways were involved in the uptake of prodrug nanoparticles. It should be noted that the fluorescence outside lysosome was much stronger than that inside the lysosome. This may facilitate the release of loaded drugs since GSH was reported to mainly distribute in the cytoplasm.[52]

The cytotoxicity of GA, GB, $^{SS}\text{CB}_{\text{GB}}$ and $^{CC}\text{CB}_{\text{GB}}$ against MB49 and NIH-3T3 cells was estimated following a standard MTT procedure. The cell growth inhibition capability of $^{SS}\text{CB}_{\text{GA}}$ and $^{CC}\text{CB}_{\text{GA}}$ in these two cell lines was also characterized to reveal the tumor selectivity of prodrug nanomedicine. As shown in Figure 3C, MB49 cells treated with GA, GB, $^{SS}\text{CB}_{\text{GB}}$, $^{SS}\text{CB}_{\text{GA}}$, $^{CC}\text{CB}_{\text{GB}}$ and $^{CC}\text{CB}_{\text{GA}}$ exhibited a concentration-dependent proliferation inhibition. GA ($0.52 \pm 0.31\mu\text{M}$), GB ($0.99 \pm 0.68\mu\text{M}$), $^{SS}\text{CB}_{\text{GA}}$ ($1.56 \pm 0.61\mu\text{M}$), $^{SS}\text{CB}_{\text{GB}}$ ($1.87 \pm 0.53\mu\text{M}$) showed similar toxicity against MB49 cells. In comparison, the toxicity of $^{CC}\text{CB}_{\text{GA}}$ ($\text{IC}_{50} = 3.69 \pm 0.71\mu\text{M}$) and $^{CC}\text{CB}_{\text{GB}}$ ($\text{IC}_{50} = 5.98 \pm 0.87\mu\text{M}$) was slightly lower ($P < 0.001$), revealing the important role of disulfide bond. The similar toxicity between GA and GB or between $^{SS}\text{CB}_{\text{GA}}$ and $^{SS}\text{CB}_{\text{GB}}$ indicated that the prodrug could be efficiently transformed into

the parent GA inside cancer cells. Compared with cancer cells, the toxicity of GB, $^{SS}CB_{GB}$ and $^{CC}CB_{GB}$ against NIH-3T3 was found to be much lower than that of GA and $^{SS}CB_{GA}$ (Figure 3D) ($P < 0.001$), which might be ascribed to the higher ROS level in tumor cells than that in normal cells.[38]

To evaluate the apoptosis of BC cells induced by the prodrug nanomedicine, MB49 cells were exposed to GA, GB, $^{CC}CB_{GA}$, $^{SS}CB_{GA}$, $^{SS}CB_{GB}$, and $^{CC}CB_{GB}$, at an equivalent GA dosage of 2 μ M for 24 h. The cells were then double stained with PI and Annexin-V FITC for viability and apoptosis assay, and analyzed by FCM. As shown in Figure 3F, the viability of MB49 cells was significantly reduced after treatment with different GA or GB formulations. Free GA contributed to 34.7% early apoptotic cells and 33.3% late apoptotic cells. While for free GB, the level was up to 33.6% and 33.7%, respectively. Slightly weaker pro-apoptotic ability was observed for the nano-formulations of both GA and GB. The results were consistent with the MTT assay in which GA and GB showed the highest toxicity. Furthermore, the influence of free drugs and nanomedicines on the cell cycle of MB49 cells was also investigated. As shown in Figure 3G, GA treatment caused a significant increase of G1 phase and decrease of S phase compared with normal cells, suggesting that the cells were arrested in G0/G1 phase by GA. Similar G1 phase increase and S phase decrease could also be observed in the rest GA or GB containing groups, further confirming that both free GB and GB nanomedicine might present the same mechanism of action as free GA and further implying the efficient transformation of GB prodrug inside cells.

3.3 Muco-adhesiveness, retention and permeation of prodrug nanomedicine in bladder

The muco-adhesiveness and permeability of free drugs and nanomedicines in bladder were confirmed by small animal living imaging system and CLSM. The tumor-bearing mice were anesthetized and then Cy7.5 labeled $^{SS}CB_{GB}$ and $^{CC}CB_{GB}$ solution at an equivalent GA dosage of 5.0 mg per kg body weight was intravesically instilled into the bladders through the urethra and stay inside bladder for 2 h. Same dosage of free Cy7.5 was used as control. At different time points after instillation

(i.e., 0, 6, 12, 24, 36, 48, and 60 hours), the mice were imaged with IVIS Spectrum living imaging system. As depicted in Figure 4A, at all time points, there was an obviously stronger fluorescence in the bladders of $^{SS}CB_{GB}$ and $^{CC}CB_{GB}$ -treated mice than that in the bladders of free Cy7.5-treated mice. The strongest Cy7.5 fluorescence was recorded at 0 h for all groups. The fluorescence intensity of free Cy7.5 decreased rapidly and became undetectable after 24 h, while the $^{SS}CB_{GB}$ and $^{CC}CB_{GB}$ -treated bladders continually showed strong fluorescence until 60 h, indicating the better muco-adhesiveness of $^{SS}CB_{GB}$ and $^{CC}CB_{GB}$ than free drugs.

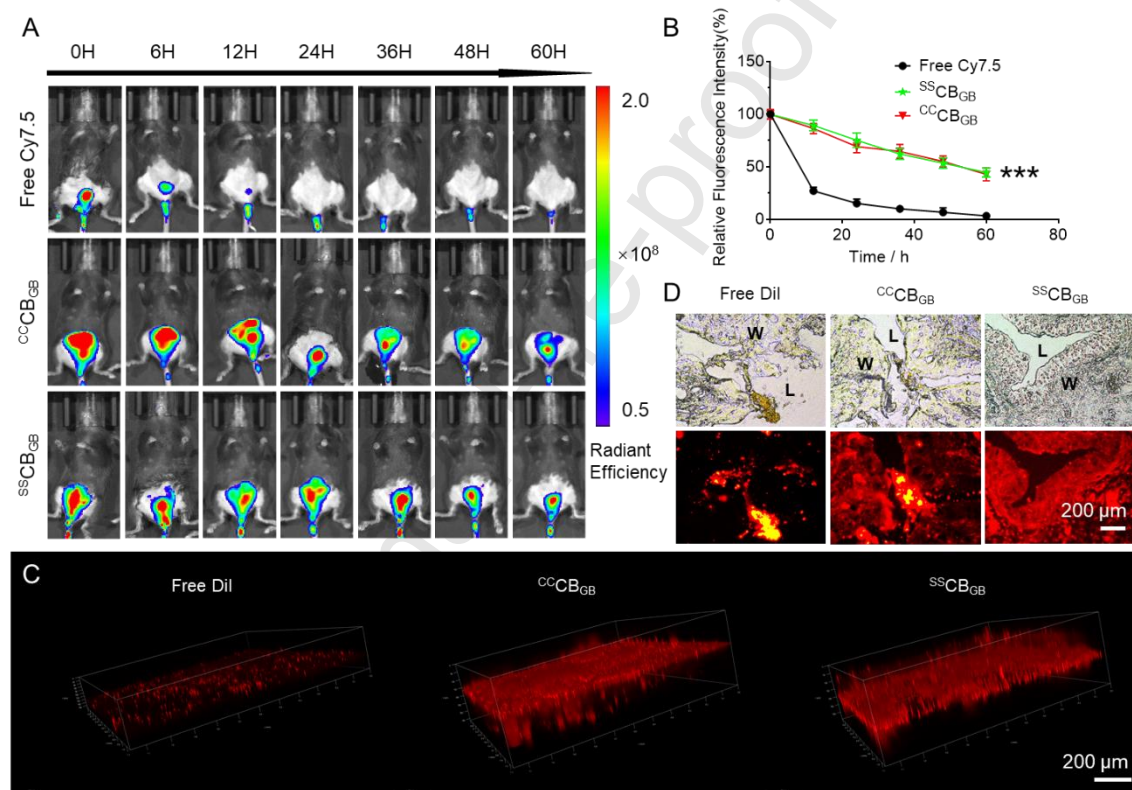


Figure 4. (A) The in vivo living imaging photographs at different time points after intravesical instillation of free Cy7.5, Cy7.5 labeled $^{SS}CB_{GB}$ and $^{CC}CB_{GB}$ for 2 h. (B) The time related fluorescent intensity changes at the bladder region of free Cy7.5, Cy7.5 labeled $^{SS}CB_{GB}$ and $^{CC}CB_{GB}$ treated mice (***P<0.001 for $^{SS}CB_{GB}$ and $^{CC}CB_{GB}$ compared with free Cy7.5, n=3). (C) The three-dimensional fluorescence distribution in the urothelium of free DiI, DiI labeled $^{SS}CB_{GB}$ and $^{CC}CB_{GB}$ nanoparticles (red) at 2 h after instillation. (D) The fluorescence distribution of DiI or DiI-labeled nanoparticles in the cross-section of bladder urothelium.

The quantitative analysis of fluorescence intensity was showed in Figure 4B. The initial fluorescence intensity of bladder at 0 h was defined as “100%”. It could be found that the fluorescence intensity of free Cy7.5 decreased rapidly after instillation, and less than 10% residual fluorescence could be observed in the bladder region at 24 h. In contrast, the excretion of nanomedicine exhibited much slower velocity. Approximately 50% residual fluorescence could still be observed for both ^{SS}CB_{GB} and ^{CC}CB_{GB} after 60 hours, which was comparable with the literature reported polypeptide nanogels.[20] Therefore, the quantitative data more convincingly confirmed the excellent muco-adhesiveness of chitosan-based nanomedicine.

To determine the permeability of free drug and positively charged nanomedicine, the penetration depth of free DiI and DiI labeled ^{SS}CB_{GB} and ^{CC}CB_{GB} nano-formulations was detected after instillation by CLSM and showed in Figure 4C & D. As observed from the 3D fluorescence distribution in the bladder wall (Figure 4C), free DiI was mainly confined near the mucous membrane in almost the entire bladder, and the largest penetration depth was found to be c.a. 40 μm. The relatively weak and punctate distributed fluorescence might be attributed to the weak muco-adhesiveness of free dye. Compared with free DiI, the nano-formulations of DiI exhibited much stronger mucous penetrating ability. Both ^{SS}CB_{GB} and ^{CC}CB_{GB} nanoparticles showed strong fluorescence with largest penetration depth reaching c.a. 200 μm, which is comparable with the reported nanogel with similar size.[20, 31] The dispersed fluorescence in the whole bladder wall could be due to the strong muco-adhesiveness of positively charged chitosan nanoparticles. However, due to the limitation of tissue transparency and laser penetration, the fluorescence distribution in deeper tissue cannot be visualized by this method. Therefore, we rechecked the mucous penetration of free dye and nano-formulations by observing the fluorescence distribution in the cross-section of bladder wall. As shown in Figure 4D, it was consistent with the 3D imaging, punctate fluorescence could be observed near the mucous membrane of free DiI treated bladder. In contrast, strong and dispersive fluorescence which extended straightly from mucous membrane to serosa could be

observed in the bladder wall of $^{SS}CB_{GB}$ and $^{CC}CB_{GB}$ groups, further revealing the adhesiveness and permeability of as-prepared prodrug nanomedicine. Overall, these phenomena indicated that the exposure to $^{SS}CB_{GB}$ and $^{CC}CB_{GB}$ could maintain a high level of drug in bladder wall, which was necessary for BC chemotherapy.

3.4 In vivo antitumor efficacy

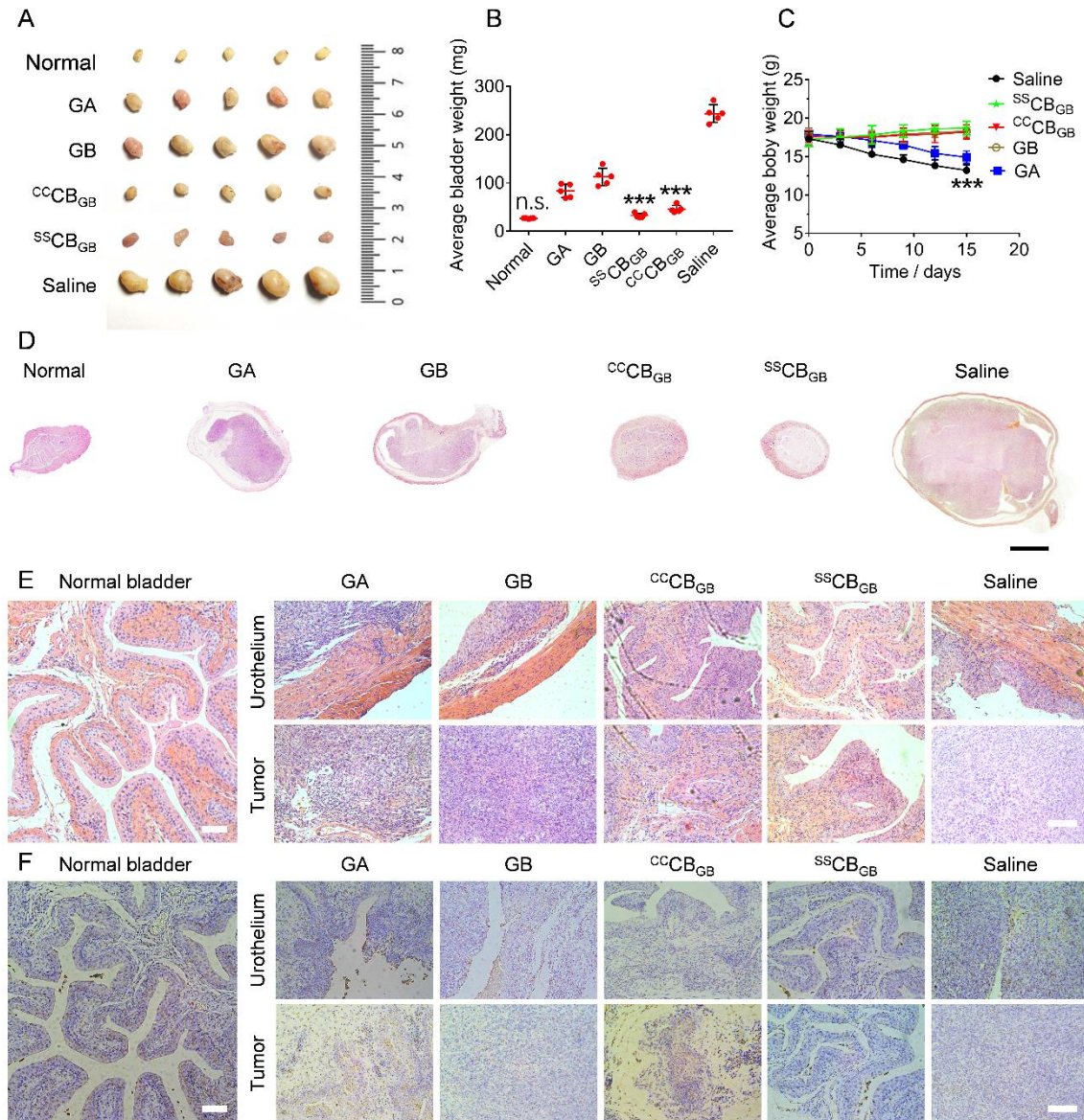


Figure 5. In vivo tumor inhibition. (A) The appearance and (B) the average weight of normal bladder and bladder treated with saline, GA, GB, $^{CC}CB_{GB}$ and $^{SS}CB_{GB}$ (** $P < 0.001$ for $^{CC}CB_{GB}$ and $^{SS}CB_{GB}$ treated bladder compared with GA, GB and saline groups; n.s. no significance for $^{SS}CB_{GB}$ compared with normal bladder). (C)

Body weight changes of tumor bearing mice during treatment with saline, GA, GB, ^{CC}CB_{GB} and ^{SS}CB_{GB} (***)P<0.001 for GA and saline compared with GB, ^{CC}CB_{GB} and ^{SS}CB_{GB}). (D) Histopathological (i.e., H&E) analyses of normal bladder and tumor tissue cross-sections after treatment with saline (as a control), GA, GB, ^{CC}CB_{GB} and ^{SS}CB_{GB}. The scale bar represents 2.5 mm. (E) The enlarged H&E micrographs of normal bladder and tumor region and urothelial region of tumor tissue cross-sections after treatment with saline (as a control), GA, GB, ^{CC}CB_{GB} and ^{SS}CB_{GB}. (F) The immunohistochemical (i.e., TUNEL) analyses of normal bladder and tumor region and urothelial region of tumor tissue cross-sections after treatment with saline (as a control), GA, GB, ^{CC}CB_{GB} and ^{SS}CB_{GB}. The scale bar in both (E) and (F) represent 100 μm.

To investigate the antitumor efficacy of various drugs in vivo, orthotopic BC xenograft models in female C57BL/6J mice were established by intravesical injection of MB49 cells after acid induced urothelium damage. To confirm whether the BC was successfully induced or not, near-infrared dye DiR labeled MB49 were injected and monitored with living imaging system at 5 days after instillation (Figure S3A). Meanwhile, the average bladder weight (Figure S3B) and histological analysis of tumor slices (Figure S3C) were investigated at 5, 10 and 15 days after tumor inoculation. The tumor bearing mice were then randomly divided into five groups (n = 5 for each group) and treated with saline, free GA, free GB, ^{CC}CB_{GB} or ^{SS}CB_{GB} at a 5.0 mg/kg dosage of GA equivalent by intravesical instillation every three day for a total of five treatments. Over the entire treatment period, the body weight was measured as an indicator of systemic toxicity. At the end of treatment, mice were anaesthetized and sacrificed, and the bladder was excised, photographed and weighed, followed by hematoxylin and eosin (H&E) staining along with major organs like heart, liver, spleen, lung and kidney. As shown in Figure 5A&B, the average weight of normal bladder as well as GA, GB, ^{CC}CB_{GB}, ^{SS}CB_{GB} and saline treated bladder was 26.5, 83.5, 113, 46.4, 31.3 and 243 mg, respectively. It was approved that both ^{CC}CB_{GB} and ^{SS}CB_{GB} could dramatically inhibit the growth of BC as compared to free

GA or GB ($P < 0.001$), which was mostly benefited from the improved muco-adhesiveness and permeability of nanoparticles. Despite the efficient in vitro anticancer activity, the suboptimal antitumor activity of free GA and GB was attributed to their quick excretion with urine. It should be noted that, both the average weight and appearance of $^{SS}CB_{GB}$ treated bladder are similar as the healthy mice bladder, which showed general weight and smooth surface. Overall, similar anticancer efficacy as the previously chitosan formulations,[25, 26] mucoadhesive[20, 31] or fluorinated formulations[32] could be obtained with as-prepared prodrug nanomedicine.

At the end of the intravesical instillation of various drugs, the bladders were excised and sectioned for histopathological examination to further verify the antitumor efficacy. For H&E staining, cancer cells were characterized by the spherical or spindle nuclei with obvious atypia compared to normal cells. However, the apoptotic cells had an ill-defined morphology, and the nuclei became darker, pyknotic, and even disappeared.[51] As shown in Figure 5D, the cross-sections of bladder treated with saline, GA and GB were filled with dense tumor mass, while $^{CC}CB_{GB}$ and $^{SS}CB_{GB}$ treated bladders exhibited similar appearance as normal bladder as revealed by intact urothelium and few cancer cells. The enlarged images of these sections could be found in Figure 5E. Large amounts of tumor cells and few tumor necrosis areas were observed in the H&E-stained tumor tissue section in the saline group, indicating the active tumor growth. Higher degrees of tumor necrosis were observed for the tumor region in GA treated bladder than that for GB, which is in accordance with the different bladder weight. Meanwhile, tumor cell infiltration into the muscular layer could also be observed in the urothelium region of GA and GB treated mice, indicating the disease progression. Encouragingly, very few tumor cell clusters could be observed in $^{CC}CB_{GB}$ treated bladder, while the tumor cells could hardly be distinguished by naked eyes in $^{SS}CB_{GB}$ treated bladder, suggesting that the muco-adhesiveness and permeability played important roles in treating BC. Except for the efficient tumor inhibition, the urothelium maintained intact after treatment with both $^{CC}CB_{GB}$ and $^{SS}CB_{GB}$. This could be explained by their “double insurance”

drug release mechanism, which led to efficient tumor cell selectivity.

Terminal deoxynucleotidyl transferase (TdT) dUTP Nick-End Labeling (TUNEL) assay has been designed to detect apoptotic cells that undergo extensive DNA degradation during the late stages of apoptosis.[53] This method is based on the ability of TdT to label blunt ends of double-stranded DNA breaks independent of a template. As shown in Figure 5F, more intense positive signal of TUNEL was observed in the GA group than in GB group, which suggested the existence of more apoptotic cells, especially in urothelial region. Since the tumor mass was almost completely eradicated by $^{CC}CB_{GB}$ and $^{SS}CB_{GB}$, the rest tissue was mainly urothelium. Therefore, the lack of apoptotic cells indicated the remarkable safety profiles of prodrug nanomedicine rather than the lack of anticancer efficacy. Moreover, immunohistochemical staining for Ki-67, which is expressed from G1 phase to anaphase and thus is suitable for estimating the fraction of a given cell population with cell-cycle activity,[54] was performed to analyze the cell proliferation status, which was shown in Figure S5. The largest number of Ki-67 positive cells was observed in the saline group, while less Ki-67 positive cells was found in the GB groups. Compare with GB, fewer Ki-67 positive cells could be observed after GA treatment, and only a few clustered proliferated tumor cells could be found for $^{CC}CB_{GB}$ treated bladder, indicating the better tumor growth inhibition. Because the rest tissue in $^{SS}CB_{GB}$ treated bladder was mainly the highly differentiated urothelial cells, no obvious cell proliferation could be observed, confirming the remarkable capability of $^{SS}CB_{GB}$ nanomedicine for BC chemotherapy. Considering the selective killing ability of the prodrug nanomedicine, the remarkable anticancer efficacy may also be attributed to the exempt of normal cells whose damage may cause the activation of a series of senescence-associated secretory phenotype (SASP) so as to promote drug resistance and tumor outgrowth.[55, 56]

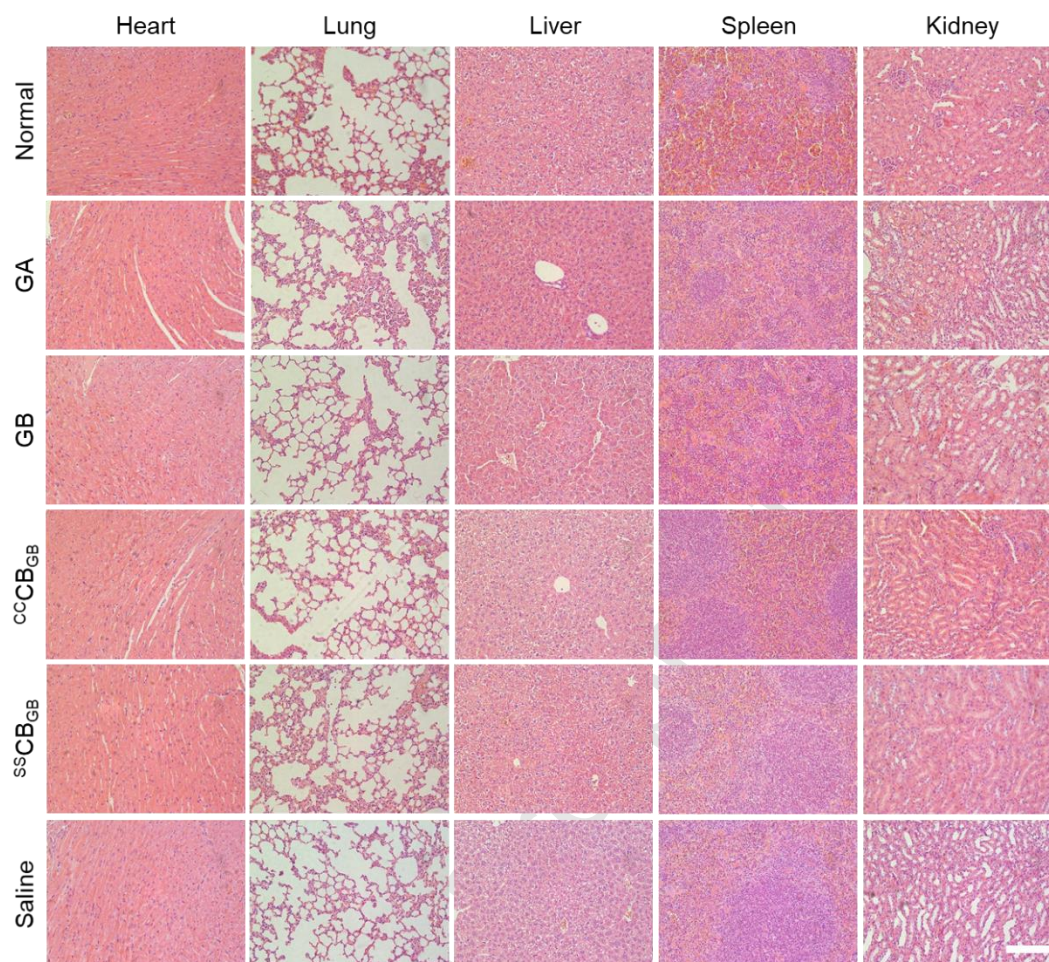


Figure 6. Histopathologic analysis of major organs including heart, lung, liver, spleen and kidney excised from normal mice or mice treated with saline, GA, GB, ^{CC}CB_{GB} and ^{SS}CB_{GB}. The scale bar represents 100 μ m.

In order to assess the toxicity of free drug and prodrug nanomedicine *in vivo*, the change in body weight was monitored after every injection. As shown in Figure 5C, during the entire process of chemotherapy, free GA and saline treated group exhibited significant weight loss. The weight loss in saline group might be due to the malignant proliferation of tumor mass which will inevitably cause the obstruction of urethra and bladder. In contrast, the weight loss after GA treatment might be explained by the sustained damage of urothelium caused by GA as indicated by the TUNEL staining of GA treated bladder (Figure 5F). The mice treated with free GB or GB nanomedicine did not show any weight loss, suggesting the negligible toxicity of prodrug strategy. Moreover, the safety of prodrug strategy can also be proved by the histopathologic

analysis of major organs like heart, liver, lung, spleen and kidney (Figure 6), in which no obvious organ toxicity could be observed for all groups. These data strongly suggested that $^{SS}CB_{GB}$ prodrug nanomedicine could efficiently adhere and penetrate bladder urothelium and selectively release GA in tumor cells, which enhanced the tumor growth inhibition effect and decreased the side effects.

4. Conclusions

In summary, a reduction- and ROS- dual responsive prodrug nanomedicine was developed for the potential intravesical chemotherapy of BC. The cationic chitosan promoted the muco-adhesiveness and penetrability of GB prodrug within the bladder wall. In addition, the reduction- and ROS-sensitive properties gave $^{SS}CB_{GB}$ the ability to accurately release GA in BC cells when compared with free drugs. Consequently, the intravesical instillation of $^{SS}CB_{GB}$ significantly inhibited tumor growth in an orthotopic BC model while caused no toxicity to normal urothelium. The safety profiles and the efficient tumor suppression in vivo demonstrate the great potential of as-prepared prodrug nanomedicine in intravesical chemotherapy.

Data availability statement

The raw/processed data required to reproduce these findings cannot be shared at this time due to technical or time limitations.

Conflict of interest

The authors declare no competing financial interest.

Acknowledgements

This work was financially supported by the National Natural Science Foundation of China (Grant Nos. 51503013, 51390481, 21774008, and 81472412) and by the long-term subsidy mechanism from the Ministry of Finance and the Ministry of Education of PRC for BUCT. This work was also supported by the Fundamental Research Funds for the Central Universities of China (Grant Nos. XK1701,

XK1802-8) and Research Projects on Biomedical Translation of China-Japan Friendship Hospital (Nos. PYBZ1823, PYBZ1838).

References

- [1] S. Chavan, F. Bray, J. Lortet-Tieulent, M. Goodman, A. Jemal, International variations in bladder cancer incidence and mortality, *Eur. Urol.* 66 (2014) 59-73.
- [2] R.G. Casey, J.W.F. Catto, L. Cheng, M.S. Cookson, H. Herr, S. Shariat, J.A. Witjes, P.C. Black, Diagnosis and management of urothelial carcinoma in situ of the lower urinary tract: A systematic review, *Eur. Urol.* 67 (2015) 876-888.
- [3] J. Ferlay, I. Soerjomataram, R. Dikshit, S. Eser, C. Mathers, M. Rebelo, D.M. Parkin, D. Forman, F. Bray, Cancer incidence and mortality worldwide: Sources, methods and major patterns in GLOBOCAN 2012, *Int. J. Cancer* 136 (2015) E359-E386.
- [4] K.D. Miller, R.L. Siegel, C.C. Lin, A.B. Mariotto, J.L. Kramer, J.H. Rowland, K.D. Stein, R. Alteri, A. Jemal, Cancer treatment and survivorship statistics, 2016, *CA-Cancer J. Clin.* 66 (2016) 271-289.
- [5] D.S. Kaufman, W.U. Shipley, A.S. Feldman, Bladder cancer, *Lancet* 374 (2009) 239-249.
- [6] O. Sanli, J. Dobruch, M.A. Knowles, M. Burger, M. Alemozaffar, M.E. Nielsen, Y. Lotan, Bladder cancer, *Nat. Rev. Dis. Primers* 3 (2017) 1-19.
- [7] S. GuhaSarkar, R. Banerjee, Intravesical drug delivery: Challenges, current status, opportunities and novel strategies, *J. Control. Release* 148 (2010) 147-159.
- [8] Z. Shen, T. Shen, M.G. Wientjes, M.A. O'Donnell, J.L.-S. Au, Intravesical treatments of bladder cancer: Review, *Pharm. Res.* 25 (2008) 1500-1510.
- [9] J.A. Witjes, K. Hendricksen, Intravesical pharmacotherapy for non-muscle-invasive bladder cancer: A critical analysis of currently available drugs, treatment schedules, and long-term results, *Eur. Urol.*, 53 (2008) 45-52.
- [10] J.Y. Fang, Z.R. Huang, Intravesical drug delivery into the bladder to treat cancers, *Curr. Drug Deliv.* 6 (2009) 227-237.
- [11] S. Wittaya-areekul, J. Kruenate, C. Prahsarn, Preparation and in vitro evaluation of mucoadhesive properties of alginate/chitosan microparticles containing prednisolone, *Int. J. Pharm.* 312 (2006) 113-118.
- [12] M. Wirth, V.E. Plattner, F. Gabor, Strategies to improve drug delivery in bladder cancer therapy, *Expert Opin. Drug Deliv.* 6 (2009) 727-744.
- [13] X. Xu, L. Guo, T. Xu, Q. Yu, Z. Gan, G. Zhang, Application of macromolecule polymer drug loading system's intravesical therapy in orthotopic bladder cancer model, *J. Clin. Urol.* 34 (2019) 895-900.
- [14] C. Rieger, D. Kunhardt, A. Kaufmann, D. Schendel, D. Huebner, K. Erdmann, S. Propping, M.P. Wirth, B. Schwenger, S. Fuessel, Characterization of different carbon nanotubes for the development of a mucoadhesive drug delivery system for intravesical treatment of bladder cancer, *Int. J. Pharm.* 479 (2015) 357-363.
- [15] D.B. Kaldybekov, P. Tonglairov, P. Opanasopit, V.V. Khutoryanskiy,

Mucoadhesive maleimide-functionalised liposomes for drug delivery to urinary bladder, *Eur. J. Pharm. Sci.* 111 (2018) 83-90.

[16] J.H. Buss, K.R. Begnini, C.B. Bender, A.R. Pohlmann, S.S. Guterres, T. Collares, F.K. Seixas, Nano-BCG: A promising delivery system for treatment of human bladder cancer, *Front. Pharmacol.* 8 (2018) 977.

[17] C. Mugabe, Y. Matsui, A.I. So, M.E. Gleave, J.H.E. Baker, A.I. Minchinton, I. Manisali, R. Liggins, D.E. Brooks, H.M. Burt, In vivo evaluation of mucoadhesive nanoparticulate docetaxel for intravesical treatment of non-muscle-invasive bladder cancer, *Clin. Cancer Res.* 17 (2011) 2788-2798.

[18] D.T. Martin, J.M. Steinbach, J. Liu, S. Shimizu, H.Z. Kaimakliotis, M.A. Wheeler, A.B. Hittelman, W.M. Saltzman, R.M. Weiss, Surface-modified nanoparticles enhance transurothelial penetration and delivery of survivin siRNA in treating bladder cancer, *Mol. Cancer Ther.* 13 (2014) 71-81.

[19] E. Bilensoy, C. Sarisozen, G. Esendağlı, A.L. Doğan, Y. Aktaş, M. Şen, N.A. Mungan, Intravesical cationic nanoparticles of chitosan and polycaprolactone for the delivery of Mitomycin C to bladder tumors, *Int. J. Pharm.* 371 (2009) 170-176.

[20] H. Guo, F. Li, W. Xu, J. Chen, Y. Hou, C. Wang, J. Ding, X. Chen, Mucoadhesive cationic polypeptide nanogel with enhanced penetration for efficient intravesical chemotherapy of bladder cancer, *Adv. Sci.* 5 (2018) 1800004.

[21] S. Lu, K.G. Neoh, E.T. Kang, R. Mahendran, E. Chiong, Mucoadhesive polyacrylamide nanogel as a potential hydrophobic drug carrier for intravesical bladder cancer therapy, *Eur. J. Pharm. Sci.* 72 (2015) 57-68.

[22] D. Zhou, G. Zhang, Z. Gan, c(RGDfK) decorated micellar drug delivery system for intravesical instilled chemotherapy of superficial bladder cancer, *J. Control. Release*, 169 (2013) 204-210.

[23] D.H. Zhou, G. Zhang, Q.S. Yu, Z.H. Gan, Folic acid modified polymeric micelles for intravesical instilled chemotherapy, *Chin. J. Polym. Sci.* 36 (2018) 479-487.

[24] Q. Yu, J. Zhang, G. Zhang, Z. Gan, Synthesis and functions of well-defined polymer-drug conjugates as efficient nanocarriers for intravesical chemotherapy of bladder cancer, *Macromol. Biosci.* 15 (2015) 509-520.

[25] O.M. Kolawole, W.M. Lau, V.V. Khutoryanskiy, Methacrylated chitosan as a polymer with enhanced mucoadhesive properties for transmucosal drug delivery, *Int. J. Pharm.*, 550 (2018) 123-129.

[26] Z.A. Şenyiğit, S.Y. Karavana, D. İlem-Özdemir, Ç. Çalışkan, C. Waldner, S. Şen, A. Bernkop-Schnürch, E. Baloğlu, Design and evaluation of an intravesical delivery system for superficial bladder cancer: Preparation of gemcitabine HCl-loaded chitosan–thioglycolic acid nanoparticles and comparison of chitosan/poloxamer gels as carriers, *Int. J. Nanomed.* 10 (2015) 6493-6507.

[27] M. Vila-Caballer, G. Codolo, F. Munari, A. Malfanti, M. Fassan, M. Rugge, A. Balasso, M. de Bernard, S. Salmaso, A pH-sensitive stearyl-PEG-poly(methacryloyl sulfadimethoxine)-decorated liposome system for protein delivery: An application for bladder cancer treatment, *J. Control. Release* 238 (2016) 31-42.

[28] P. Bassi, A. Volpe, D. D'Agostino, G. Palermo, D. Renier, S. Franchini, A. Rosato, M. Racioppi, Paclitaxel-hyaluronic acid for intravesical therapy of bacillus

Calmette-Guerin refractory carcinoma in situ of the bladder: Results of a phase I study, *J. Urol.* 185 (2011) 445-449.

[29] M. Eroglu, E. Öztürk, N. Özdemir, E.B. Denkbapi, I. Doğan, A. Acar, M. Güzel, Mitomycin-C-loaded alginate carriers for bladder cancer chemotherapy: in vivo studies, *J. Bioact. Compat. Polym.* 20 (2005) 197-208.

[30] C.W. Liu, L.C. Chang, K.J. Lin, T.J. Yu, C.C. Tsai, H.K. Wang, T.R. Tsai, Preparation and characterization of gelatin-based mucoadhesive nanocomposites as intravesical gene delivery scaffolds, *Biomed Res. Int.* 2014 (2014) 473823.

[31] H. Guo, W. Xu, J. Chen, L. Yan, J. Ding, Y. Hou, X. Chen, Positively charged polypeptide nanogel enhances mucoadhesion and penetrability of 10-hydroxycamptothecin in orthotopic bladder carcinoma, *J. Control. Release* 259 (2017) 136-148

[32] G. Li, Q. Lei, F. Wang, D. Deng, S. Wang, L. Tian, W. Shen, Y. Cheng, Z. Liu, S. Wu, Fluorinated polymer mediated transmucosal peptide delivery for intravesical instillation therapy of bladder cancer, *Small* 15 (2019) 1900936.

[33] E.A. Mun, A.C. Williams, V.V. Khutoryanskiy, Adhesion of thiolated silica nanoparticles to urinary bladder mucosa: Effects of PEGylation, thiol content and particle size, *Int. J. Pharm.*, 512 (2016) 32-38.

[34] J. Barthelmes, S. Dünnhaupt, S. Unterhofer, G. Perera, W. Schlocker, A. Bernkop-Schnürch, Thiolated particles as effective intravesical drug delivery systems for treatment of bladder-related diseases, *Nanomedicine* 8 (2013) 65-75.

[35] C. Mugabe, B.A. Hadaschik, R.K. Kainthan, D.E. Brooks, A.I. So, M.E. Gleave, H.M. Burt, Paclitaxel incorporated in hydrophobically derivatized hyperbranched polyglycerols for intravesical bladder cancer therapy, *BJU Int.* 103 (2010) 978-986.

[36] C. Huang, K.G. Neoh, L. Xu, E.T. Kang, E. Chiong, Polymeric nanoparticles with encapsulated superparamagnetic iron oxide and conjugated cisplatin for potential bladder cancer therapy, *Biomacromolecules* 13 (2012) 2513-2520.

[37] K. Hendricksen, D. Gleason, J.M. Young, D. Saltzstein, A. Gershman, S. Lerner, J.A. Witjes, Safety and side effects of immediate instillation of apaziquone following transurethral resection in patients with nonmuscle invasive bladder cancer, *J. Urol.* 180 (2008) 116-120.

[38] S. Prasad, S.C. Gupta, A.K. Tyagi, Reactive oxygen species (ROS) and cancer: Role of antioxidative nutraceuticals, *Cancer Lett.* 387 (2017) 95-105.

[39] K. Shimada, T. Fujii, S. Anai, K. Fujimoto, N. Konishi, ROS generation via NOX4 and its utility in the cytological diagnosis of urothelial carcinoma of the urinary bladder, *BMC Urol.* 11 (2011) 22.

[40] F. Meng, W.E. Hennink, Z. Zhong, Reduction-sensitive polymers and bioconjugates for biomedical applications, *Biomaterials* 30 (2009) 2180-2198.

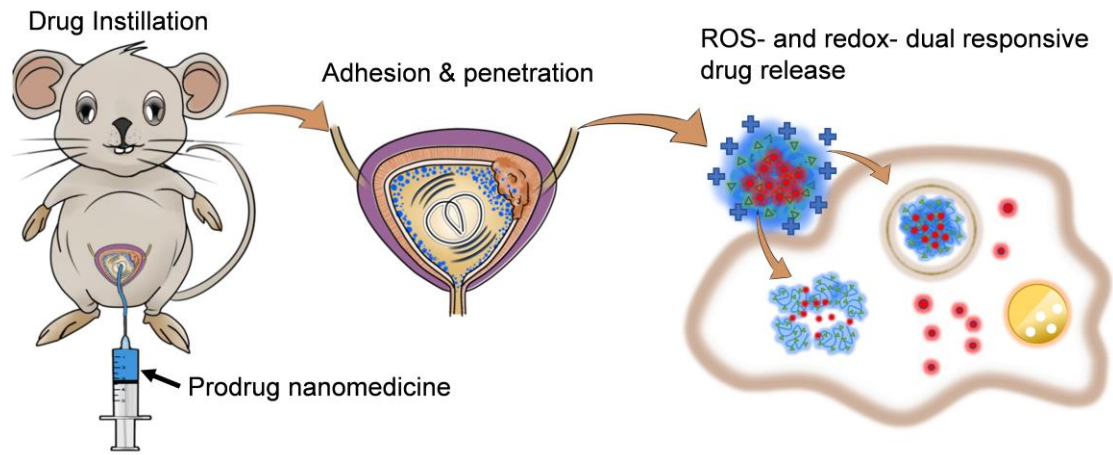
[41] Y. Zhu, J. Zhang, F. Meng, C. Deng, R. Cheng, J. Feijen, Z. Zhong, cRGD-functionalized reduction-sensitive shell-sheddable biodegradable micelles mediate enhanced doxorubicin delivery to human glioma xenografts in vivo, *J. Control. Release* 233 (2016) 29-38.

[42] V.V. Khutoryanskiy, Advances in mucoadhesion and mucoadhesive polymers, *Macromol. Biosci.* 11 (2011) 748-764.

- [43] D. Kashyap, R. Mondal, H.S. Tuli, G. Kumar, A.K. Sharma, Molecular targets of gambogic acid in cancer: Recent trends and advancements, *Tumor Biology* 37 (2016) 12915-12925.
- [44] H. Tang, J. Tang, Y. Shen, W.X. Guo, M. Zhou, R.H. Wang, N. Jiang, Z.H. Gan, Q.S. Yu, Comb-like poly(N-(2-hydroxypropyl) methacrylamide) doxorubicin conjugates: The influence of polymer architecture and composition on the biological properties, *Chin. J. Polym. Sci.* 36 (2018) 1225-1238.
- [45] O.M. Kolawole, W.M. Lau, H. Mostafid, V.V. Khutoryanskiy, Advances in intravesical drug delivery systems to treat bladder cancer, *Int. J. Pharm.* 532 (2017) 105-117.
- [46] D. Trachootham, J. Alexandre, P. Huang, Targeting cancer cells by ROS-mediated mechanisms: A radical therapeutic approach?, *Nat. Rev. Drug Discov.* 8 (2009) 579-591.
- [47] Y. Kuang, K. Balakrishnan, V. Gandhi, X. Peng, Hydrogen peroxide inducible DNA cross-linking agents: Targeted anticancer prodrugs, *J. Am. Chem. Soc.* 133 (2011) 19278-19281.
- [48] K.E. Broaders, S. Grandhe, J.M. Fréchet, A biocompatible oxidation-triggered carrier polymer with potential in therapeutics, *J. Am. Chem. Soc.* 133 (2010) 756-758.
- [49] X. Liu, J. Xiang, D. Zhu, L. Jiang, Z. Zhou, J. Tang, X. Liu, Y. Huang, Y. Shen, Fusogenic reactive oxygen species triggered charge- reversal vector for effective gene delivery, *Adv. Mater.* 28 (2016) 1743-1752.
- [50] M. Ye, Y. Han, J. Tang, Y. Piao, X. Liu, Z. Zhou, J. Gao, J. Rao, Y. Shen, A tumor- specific cascade amplification drug release nanoparticle for overcoming multidrug resistance in cancers, *Adv. Mater.* 29 (2017) 1702342.
- [51] X. Yan, Q. Yu, L. Guo, W. Guo, S. Guan, H. Tang, S. Lin, Z. Gan, Positively charged combinatory drug delivery systems against multi-drug-resistant breast cancer: Beyond the drug combination, *ACS Appl. Mater. Interfaces* 9 (2017) 6804-6815.
- [52] T. Yin, J. Liu, Z. Zhao, Y. Zhao, L. Dong, M. Yang, J. Zhou, M. Huo, Redox sensitive hyaluronic acid- decorated graphene oxide for photothermally controlled tumor- cytoplasm- selective rapid drug delivery, *Adv. Funct. Mater.* 27 (2017) 1604620.
- [53] K. Kyrylkova, S. Kyryachenko, M. Leid, C. Kioussi, Detection of apoptosis by TUNEL assay, *Methods Mol. Biol. (N. Y.)*, 887 (2012) 41-47.
- [54] T. Scholzen, J. Gerdes, The Ki-67 protein: From the known and the unknown, *J. Cell. Physiol.* 182 (2000) 311-322.
- [55] Y. Sun, J. Campisi, C. Higano, T.M. Beer, P. Porter, I. Coleman, L. True, P.S. Nelson, Treatment-induced damage to the tumor microenvironment promotes prostate cancer therapy resistance through WNT16B, *Nat. Med.* 18 (2012) 1359-1368.
- [56] A. Georgilis, J. Gil, Controlling secretion to limit chemoresistance, *Genes Dev.* 30 (2016) 1791-1792.

Xin Xu: Investigation, Methodology, Writing- Original draft preparation. **Kunpeng Liu:** Investigation, Writing- Original draft preparation. **Binbin Jiao:** Investigation. **Kejun Luo:** Investigation. **Jian Ren:** Validation. **Guan Zhang:** Supervision, Funding acquisition. **Qingsong Yu:** Conceptualization, Supervision, Writing- Reviewing and Editing, Funding acquisition. **Zihua Gan:** Supervision, Funding acquisition.

Journal Pre-proof



Journal Pre-proof

Highlights,

- Mucoadhesive nanoparticles enhanced the retention of drugs in bladder;
- The positive nature improved the penetration of nanoparticles inside urothelium;
- ROS- and redox- dual responsive nanoparticles selectively killed cancer cells;
- Prodrug nanoparticles caused significant tumor inhibition and negligible side effect.

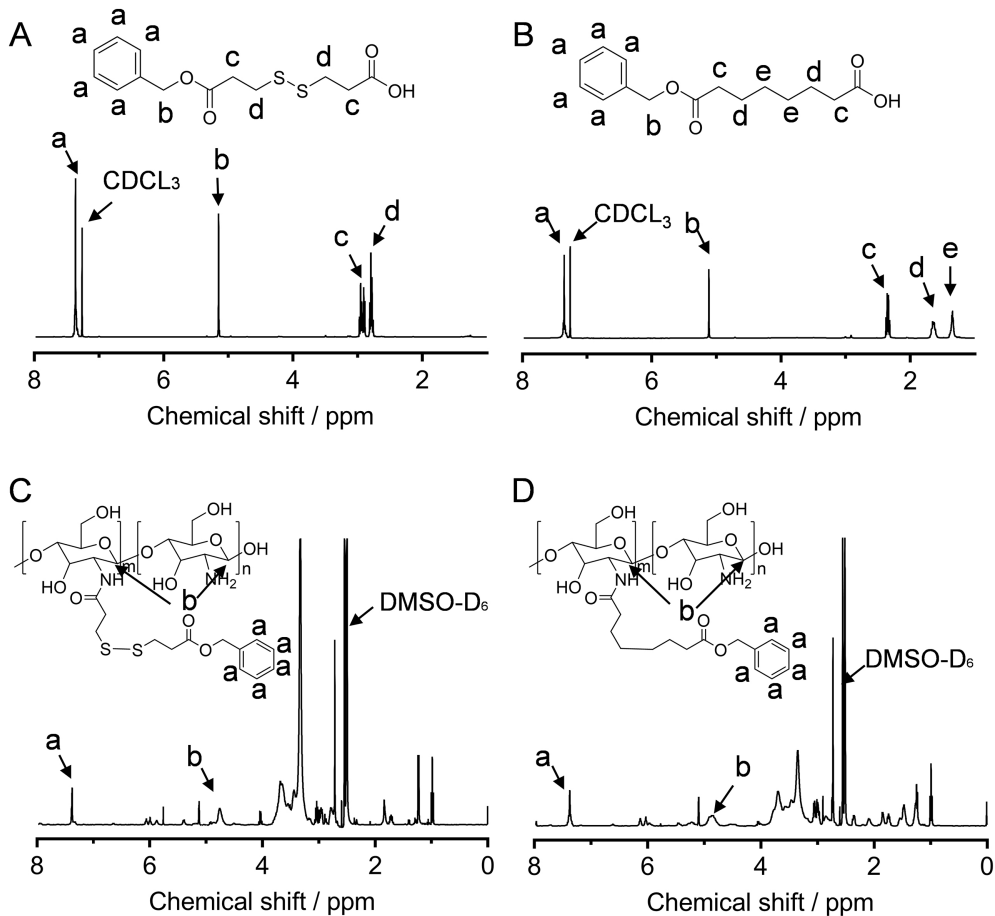


Figure 1

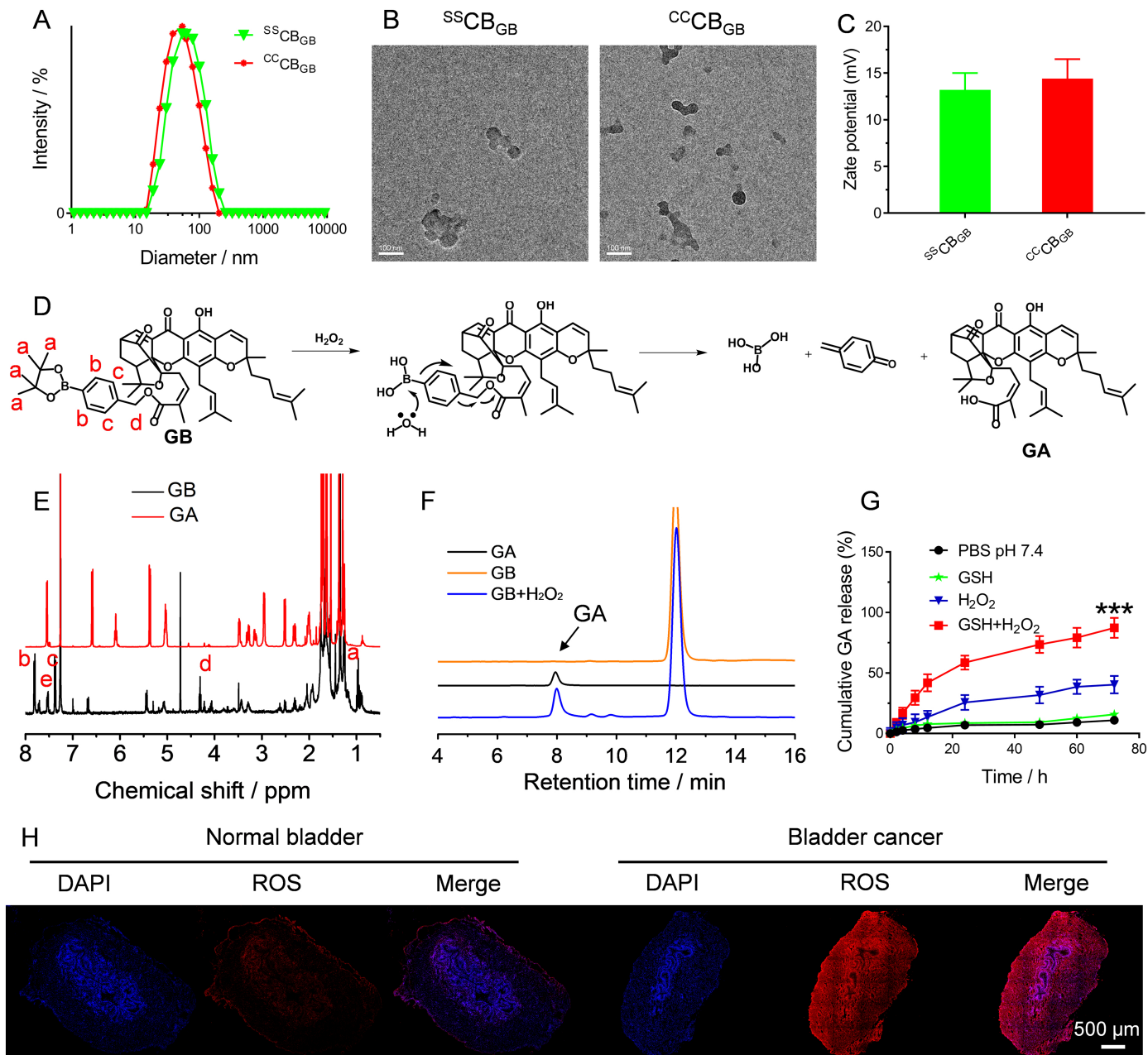


Figure 2

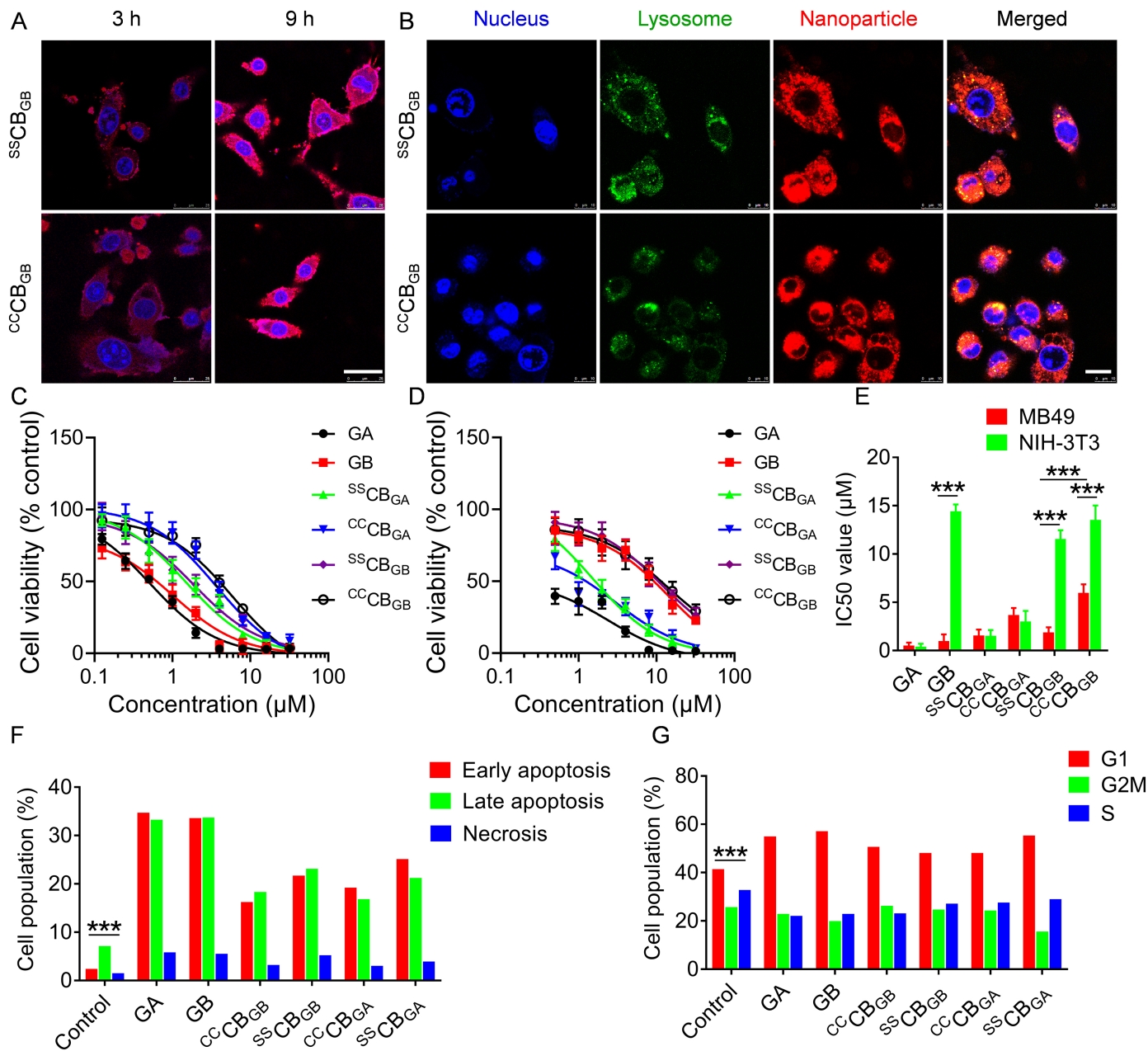


Figure 3

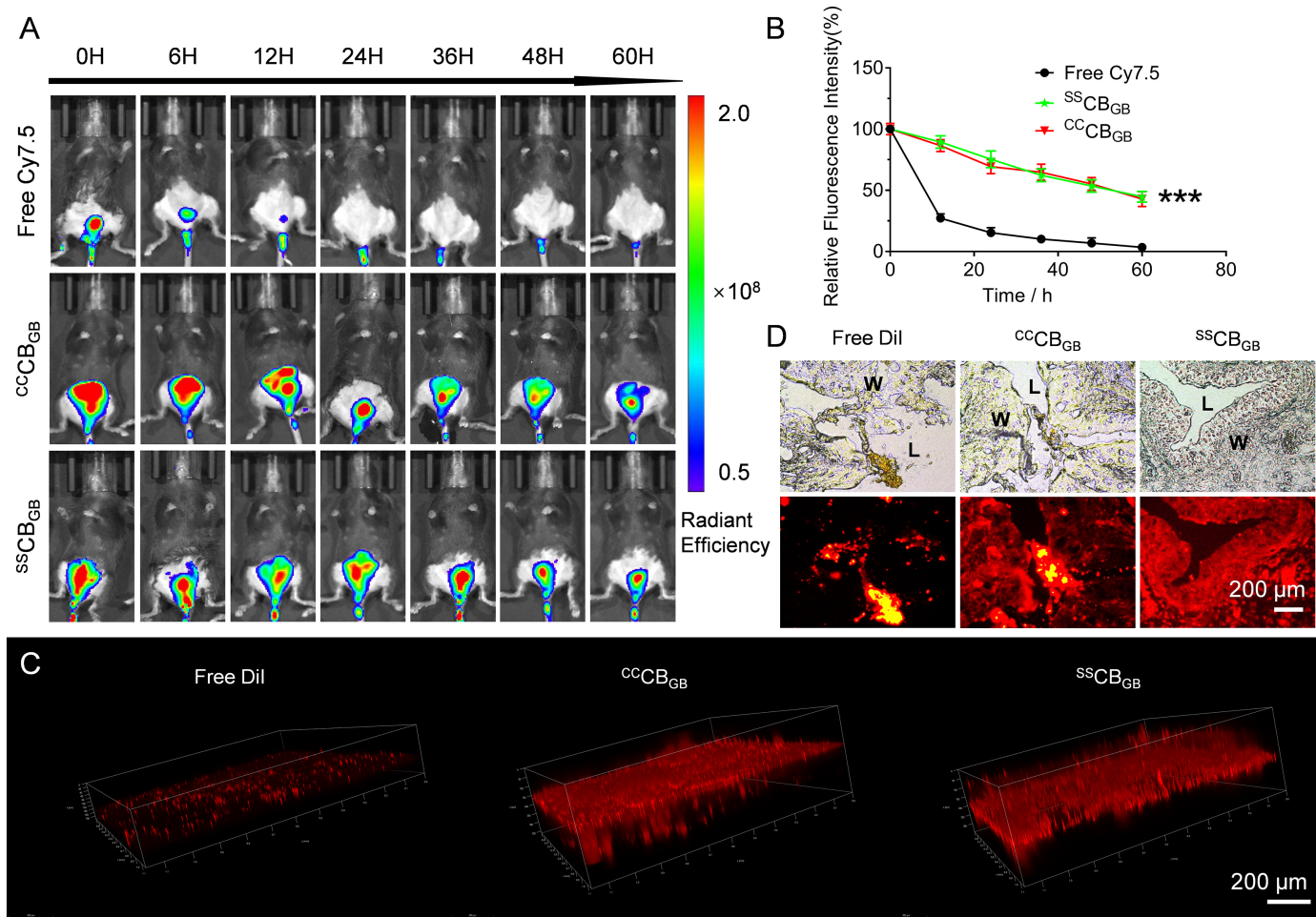


Figure 4

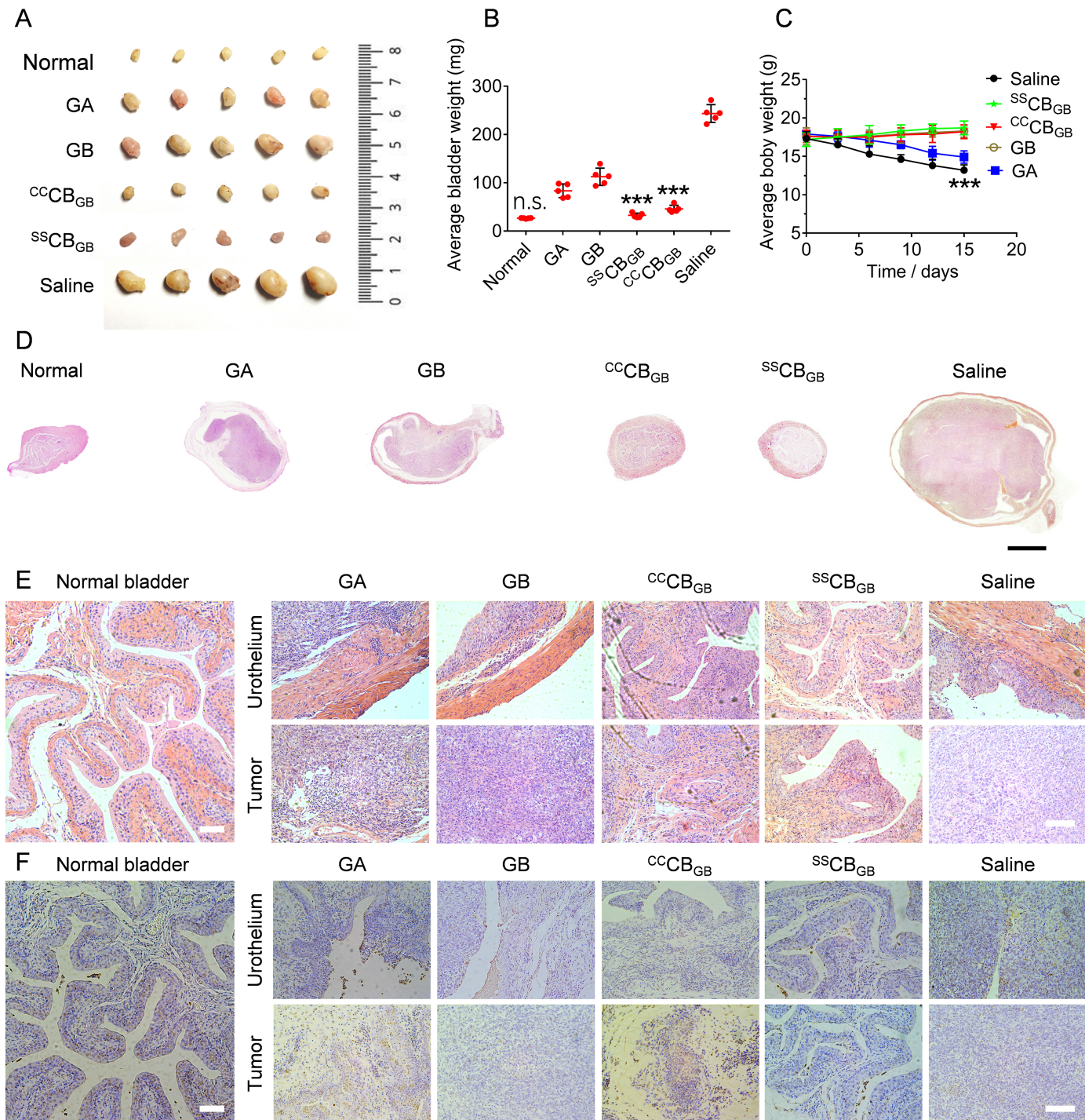


Figure 5

Heart

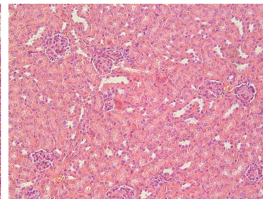
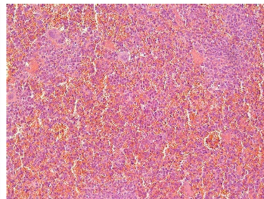
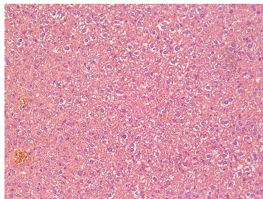
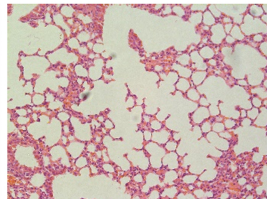
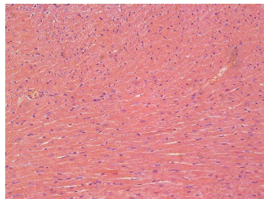
Lung

Liver

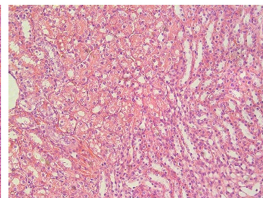
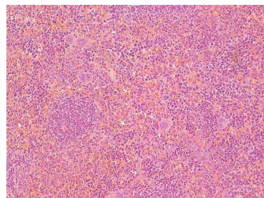
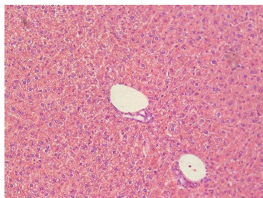
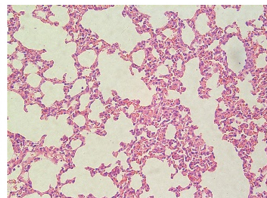
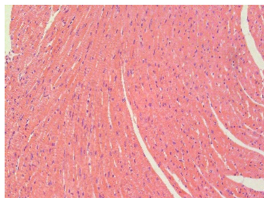
Spleen

Kidney

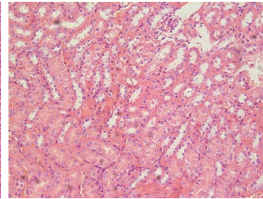
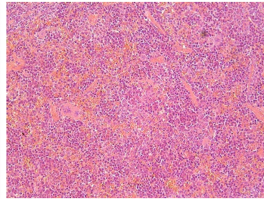
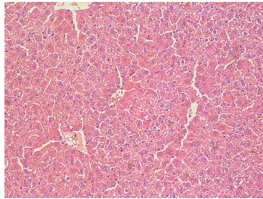
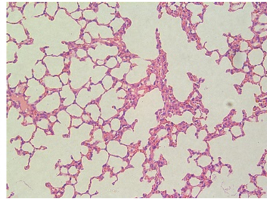
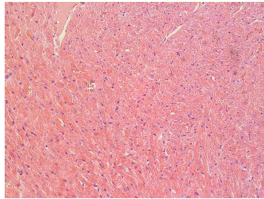
Normal



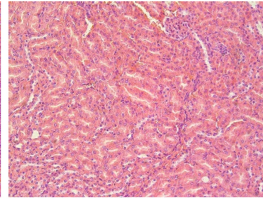
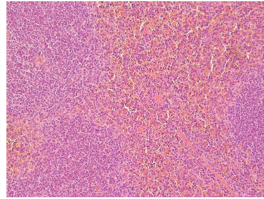
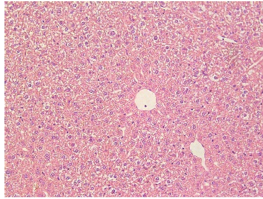
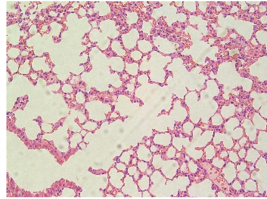
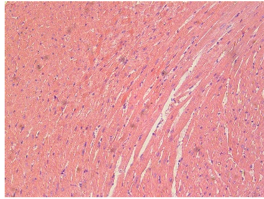
GA



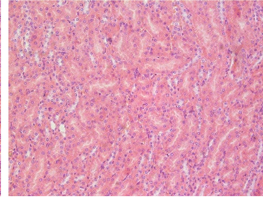
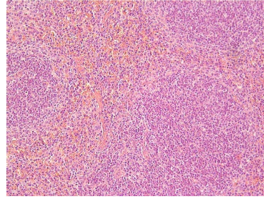
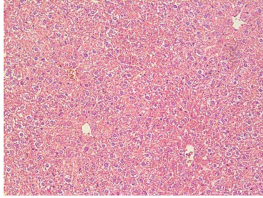
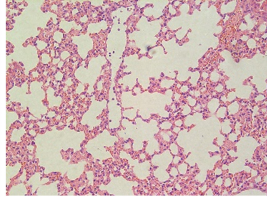
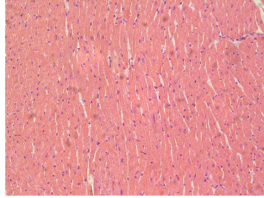
GB



CCCB_{GB}



SSCB_{GB}



Saline

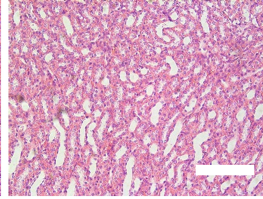
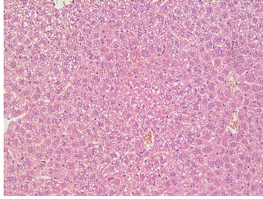
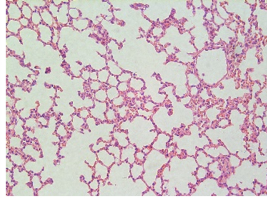
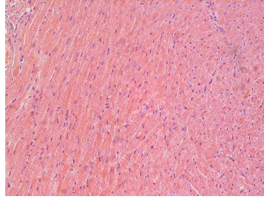


Figure 6